Multiphoton absorption at metal alkynyl complexes

Ling Zhang and Mark G. Humphrey*

Research School of Chemistry, Australian National University

Canberra, ACT 2601, Australia

L.Z.: linda.x.zhang@anu.edu.au

M.G.H.: Mark.Humphrey@anu.edu.au

Contribution to the Special Issue of Coordination Chemistry Reviews

for the 8th Asian Conference on Coordination Chemistry (ACCC8)

* Correspondence to:

Professor M. G. Humphrey

Research School of Chemistry

Australian National University

Canberra, ACT 2601

Australia

Email: Mark.Humphrey@anu.edu.au

Abstract:

Materials exhibiting multi-photon absorption (MPA) are of significant interest for a range of applications including microfabrication, bio-imaging and sensing, and photodynamic therapy. Amongst the possible MPA materials, metal alkynyl complexes have attracted significant recent interest because the collinear metal and alkynyl ligand promote strong electron delocalization and intra-molecular charge transfer, resulting in complexes that can display outstanding MPA behavior. This review summarizes recent progress with metal alkynyl complexes as potential MPA materials, with an emphasis on structure-MPA property relationships that signpost the route to efficient multi-photon absorbers. A brief introduction to the theory of nonlinear optics that underpins MPA and an overview of the key experimental techniques to determine molecular MPA properties are also provided.

(insert TOC graphic here)

Keywords

Multi-photon absorption, metal alkynyl complex, metal acetylide complex, organometallic complex, dendrimer

Abbreviations

2PA	two-photon absorption
2PEF	two-photon excited fluorescence
3PA	three-photon absorption
4PA	four-photon absorption
5PA	five-photon absorption
Cy	cyclohexyl
DC	direct current
dppe	1,2-bis(diphenylphosphino)ethane
MOFs	metal-organic frameworks
MPA	multi-photon absorption
MPEF	multi-photon excited fluorescence
NLO	nonlinear optical
nPA	n-photon absorption for an integer n
OPE	oligo(*p*-phenyleneethynylene)
OPV	oligo(*p*-phenylenevinylene)
PE	*p*-phenyleneethynylene
PV	*p*-phenylenevinylene

Contents

1. Introduction
2. NLO theory
3. MPA measurements
    3.1. Direct methods
    3.2. Indirect methods
4. MPA-active metal alkynyl complexes
    4.1. Two-photon absorption at metal alkynyl complexes
        4.1.1 Dipolar metal alkynyl complexes
        4.1.2 Quadrupolar and centrosymmetric metal alkynyl complexes
        4.1.3 Octupolar metal alkynyl complexes and dendrimers
    4.2. Higher-order multi-photon absorption at metal alkynyl complexes
5. Conclusion and perspectives

Conflicts of interest

Acknowledgements

References

1. Introduction

Nonlinear optics is the discipline that describes fundamental interactions between matter and light, especially intense light; it is important for applications in signal processing, optical computing, ultrafast switching, sensing, laser amplification, etc. [1-3]. Nonlinear optical (NLO) effects were first recognized in the late 19th century, when the refractive indexes of certain solids and liquids were observed to change on application of a strong DC field; the samples became birefringent, with different light polarizations (parallel or perpendicular to the applied electric field) [4,5]. This Kerr electro-optic effect is described by:

$$\Delta n = \lambda K E^2 \quad (1)$$

where Δn is the difference in the refractive indexes of the material in the absence of a field and the presence of the DC field, λ is the wavelength of the light, K is the Kerr constant, and E is the strength of the applied electric field. A similar effect, the Pockels electro-optic effect, corresponds to birefringence changes proportional to an electric field [6]. These studies highlighted the unexplored world of nonlinear optics before the invention of the laser [7]. The first laser-based NLO experiment used the intense monochromatic light from a ruby laser, producing a second-harmonic response from crystalline quartz [8], and marking the origin of nonlinear optics as a new separate scientific subfield [7].

The increasing availability of lasers paved the way for the demonstration of many NLO effects including multi-photon absorption (MPA), and then drove the subsequent application of NLO-active materials in a wide range of fields. For example, materials possessing strong nonlinear absorption properties have great potential as optical limiters in personal protection equipment [9-13] and in the protection of delicate devices [14-17], in the control of the pulse duration of lasers [18,19] and in mode-locking lasers [20-22], and in the provision of spectroscopic information [23,24]. MPA-active materials are also increasingly important in technologies such as three-dimensional imaging, printing, switching, and fabrication [25,26], because the intrinsic spatial confinement of MPA enhances contrast and resolution. MPA can proceed by excitation at wavelengths in the near-infrared region in the vicinity of 800 nm, which corresponds to the maximum transparency of biological materials such as tissue, and this is beneficial to imaging [27,28], sensing, and therapy applications [29-38]. MPA materials can also be used in signal attenuation and telecommunications, including up-conversion and down-conversion [39], because a quadratic or higher-order dependence on the incident light intensity leads to tight spatial control of the excitation volume. In symmetric species, even-order MPA can access different excited states to those accessed from linear absorption, due to different selection rules. Furthermore, because visible or ultraviolet photons can initiate certain chemical reactions, MPA has been applied in ultra-fast surface reactions, surface dynamics, surface magnetization, and photocatalysis [40].

With most organic and coordination complex chromophores, two-photon absorption (2PA) occurs in the visible or near-infrared region, which is frequently a spectroscopic "window", greatly facilitating measurement. However, longer wavelengths are also of applications interest, and with the advent of dedicated optical parametric amplifiers and high energy/short pulse length laser technology, studies of three-photon (3PA), four-photon (4PA), five-photon (5PA), and even higher-order nonlinear absorption have increased [41,42], with both theoretical [43-48] and applied emphases [49-55]. In this review, we focus on the nonlinear absorption properties of metal alkynyl complexes, with an emphasis on progress with 2PA over the past twelve years and a summary of multi-photon absorption (nPA, $n > 2$) studies. A brief overview of the underpinning theory is also provided to clarify the discussion. The advantages and disadvantages of the key techniques employed to characterize the performance of MPA-active molecules are also described.

2. NLO theory

Nonlinear optical (NLO) effects result from the interactions of intense light with media or at the interface between media. The electromagnetic fields of the incident radiation interact with matter and other light waves, resulting in changes in frequency, phase, polarization, or path of the incident light [1,56,57]. Electromagnetic radiation interacts with matter via its electrical and magnetic fields, but in most cases, only the electrical component is important. At the molecular level, when the electrical field of the radiation is incident on a molecule, it can distort the electron density distribution of the molecule. This instantaneous change, which is the polarization of the molecule (μ), can be described as:

$$\text{Polarization } (\mu) = \mu_0 + \alpha E_{loc} + \beta E_{loc} E_{loc} + \gamma E_{loc} E_{loc} E_{loc} + \ldots \quad (2)$$

(where Taylor series factorials have been absorbed into the coefficients (the perturbation series or B convention)). The polarization of a molecule is a vector and is a function of the local electric field E_{loc}. The tensor α is the linear polarizability and the tensors β and γ are the quadratic hyperpolarizability (a $3 \times 3 \times 3$ matrix) and the cubic hyperpolarizability (a $3 \times 3 \times 3 \times 3$ matrix), respectively, while μ_0 is the static dipole (the dipole in the absence of an electric field) [56]. For a relatively weak electric field, the polarization of a molecule varies approximately linearly with changes in the local field. However, this approximation does not remain valid with increasing electric field strength, as the higher-order terms become important. These terms beyond αE_{loc} are not linear with the electric field; they result in nonlinear polarization and NLO effects, but because $\alpha >> \beta$ and γ, few NLO effects were observed before the invention of the laser.

From the macroscopic perspective, the nonlinear polarization of a material can be written as:

$$\text{Polarization (P)} = P_0 + \chi^{(1)}E + \chi^{(2)}EE + \chi^{(3)}EEE + \ldots \quad (3)$$

where P_0 is the intrinsic polarization of the material, $\chi^{(n)}$ is the *n*-th order susceptibility, and E is the electric field [56]. For media that display inversion symmetry, even-order susceptibilities vanish under the electric dipole approximation, so when the electric field of light is a single input frequency, and employing a trigonometric functional expression, $E(t) = E_0\cos(\omega t)$, to account for the oscillating electric field of a light wave, equation (3) can be rewritten for a centrosymmetric and isotropic material as:

$$P(t) = P_0 + \chi^{(1)}E_0\cos(\omega t) + \chi^{(3)}E_0^3\cos^3(\omega t) + \chi^{(5)}E_0^5\cos^5(\omega t) + \ldots \quad (4)$$

where the imaginary part of $\chi^{(3)}$ is related to the 2PA process and the real part is related to the nonlinear refraction process. The fourth term in equation (4) involves the fifth-order nonlinear susceptibility, $\chi^{(5)}$, which is also a complex quantity with its imaginary part related to the three-photon absorption (3PA) process. In general, *n*-photon absorption (nPA) corresponds to a resonant (2*n*-1)-th order nonlinear process.

2PA is a third-order NLO phenomenon, in which a molecule simultaneously absorbs two photons and is excited from the ground state to a higher energy state (the excited state). 2PA can only be achieved if the energy of the photon is at least half the energy-gap between the ground state and the excited state. 2PA was predicted theoretically thirty years before its experimental verification in the 2PA-induced frequency-upconversion fluorescence of a europium-doped crystal [58,59]. The unit for the molecular 2PA cross-section is the Göppert-Mayer (GM), where 1 GM = 10^{-50} cm^4 s $photon^{-1}$ [60]. Due to the advantages of high directionality, high monochromaticity, high intensity, and the tunability of coherent radiation from various types of laser devices, it is now in principle possible to observe not only 2PA, but also 3PA, 4PA, 5PA, and higher-order MPA-related processes; the key requirement remains the need to engineer sufficiently high molecular MPA cross-sections.

3. MPA measurements

As previously discussed, the MPA properties of materials are of rapidly increasing interest for a number of photonic and optoelectronic applications, so considerable effort has been made to determine the MPA cross-sections of chromophores in order to develop structure-property relationships that could be applied to the rational design of novel MPA-active materials. The determination of the order (the "n" in nPA) and the magnitude of MPA can be conducted by

either a direct method or an indirect method [42]. In an MPA process, a certain number of photons is absorbed simultaneously to excite a molecule or a material from the ground state to the excited state (**Fig. 1**). The direct method involves probing the transmitted pulsed energy as a function of wavelength, to determine the MPA cross-section and the number of photons. Indirect methods such as multiphoton-excited fluorescence (MPEF) rely on measuring an observable quantity in the system (in this case fluorescence) to ascertain MPA. During MPEF, the power relationship between the output intensity of the fluorescence and the input light intensity is examined, to determine the number of photons absorbed in the process; MPEF is only possible with materials exhibiting significant fluorescence and minimal scattering [61-63].

(insert Figure 1 here)

3.1 Direct methods

The imaginary part of the NLO process, nonlinear absorption, can be considered as the optical loss with the propagation of light, during which a number of photons have been absorbed by a medium. The direct method of determining MPA cross-section is to measure the deviation in material absorption from linearity as the light intensity is increased. There are a few approaches to conduct such measurements (e.g. the nonlinear transmission technique). However, the most common way of quantifying the nonlinear absorption properties is the Z-scan technique, which measures the absolute values of the nonlinear absorption and nonlinear refraction in a single experiment [64-67].

Multi-photon absorption occurs when intense light passes through an MPA-active medium, during which two or more photons are simultaneously absorbed by the material. For an absorptive nonlinearity, the light field induces an intensity-dependent absorption that can be expressed as:

$$\alpha = \alpha_0 + \alpha_2 I + \alpha_3 I^2 + \alpha_4 I^3 + \alpha_5 I^4 + \ldots \quad (5)$$

where α_0 is the linear absorption coefficient of the medium, and α_2, α_3, α_4, and α_5 are the two-, three-, four- and five-photon absorption coefficients, respectively. If only one nonlinear process takes place, which can be achieved by selecting an appropriate excitation wavelength in a spectral region in which the sample exhibits negligible linear absorption, the change in irradiance with distance in the sample can be described as:

$$dI(z,r,t)/dz = -\alpha_n I^n(z,r,t) \quad (6)$$

where I is the light intensity at the sample surface, z is the propagation distance, α_n is the n-

photon absorption coefficient, and n is the number of absorbed photons. In a simplified formulation, equation (6) can be integrated over area and time for a homogeneous sample and a temporally Gaussian pulse (TEM_{00}), allowing the determination of the normalized energy transmittance for the 2PA, 3PA, 4PA, and 5PA processes. The normalized open-aperture Z-scan transmittance, $T(z)$, can be calculated according to:

$$T(z) = \frac{\iint I(z,r,t)dAdt}{\iint I_i(z,r,t)dAdt} \quad (7)$$

By fitting the Z-scan experimental curves, the nonlinear absorption coefficient, α_n, can be obtained and converted to the n-photon absorption cross-section, σ_n, via the following equation:

$$\sigma_n = \alpha_n(h\nu)^{n-1}/N_0 \quad (8)$$

with N_0 being the concentration of absorbing species per cm^3, and $h\nu$ the photon energy.

In a typical Z-scan setup (**Fig. 2**), a wavelength-tunable laser beam is passed through a neutral density filter (to attenuate the laser beam, and thereby avoid damage to the sample solution), and is then split into two beams via a beamsplitter, with one beam reflected to the reference detector that monitors and records the incident light intensity (S_r) and the second beam directed towards a focal lens to generate the nonlinear effects. The sample cell (with pathlength normally ca. 1 mm) is sited on a motorized linear translation stage, so that it can change its position with regards to the focal plane of the lens which is located at position z_0. In the far field after passing through the focal point, the transmitted light through the sample solution is split into two parts. One part is reflected towards a focal lens, collected, and then focused onto the open-aperture detector to record the transmittance (S_o). The second part is passed through a pinhole and then to the closed-aperture detector to record the transmittance (S_c). As the sample solution travels along the beam path and through the focal region, the corresponding transmittances (reference signal and open- and closed-aperture transmittances) are recorded as Z-scan traces for data analysis. The laser intensity reference signal (S_r), open-aperture transmittance (S_o), and closed-aperture transmittance (S_c) are recorded as a function of the sample solution position (z) relative to the laser beam focal point z_0.

(insert Figure 2 here)

The traces shown in **Fig. 2** are idealized; measurements of intensity as a function of position z should ideally appear similar to these model traces. The measurements start far from the focus (negative z), where the transmittance is relatively constant; the sample then moves towards the focal point, and then to positive z. With closed-aperture detection, if the material has a positive nonlinear refraction ($n_2 > 0$), the transmittance (S_c) graph has a valley first and then a peak (see self-focussing trace). If the material has a negative refractive nonlinearity ($n_2 < 0$), then the

graph is the opposite, with first the peak and then the valley (see self-defocussing trace). With open-aperture detection, if the sample displays nonlinear absorption, the graph of the transmittance (S_o) shows a symmetric valley. From the Z-scan data, one can construct two normalized transmittances, T_o and T_c:

$$T_o = S_o(z)/S_r(z);\ T_c = S_c(z)/S_o(z) \tag{9}$$

where T_o is associated with nonlinear absorption and T_c is associated with nonlinear refraction.

As mentioned before, the Z-scan technique is often used to measure the third-order nonlinear susceptibility of materials, $\chi^{(3)}$. There are two components to the $\chi^{(3)}$ tensor, namely, the real part $\chi_r^{(3)}$ from the nonlinear refraction, and the imaginary part $\chi_i^{(3)}$ that is linked to the nonlinear absorption:

$$\chi^{(3)} = \chi_r^{(3)} + i\chi_i^{(3)} \tag{10}$$

In SI units, the above parameters are related to $\chi^{(3)}$ via:

$$\chi_r^{(3)} = 4/3n_0^2\varepsilon_0 c_0 n_2;\ \chi_i^{(3)} = \lambda/(3\pi)n_0^2\varepsilon_0 c_0\alpha_2 \tag{11}$$

where λ is the wavelength, ε_0 is the permitivity of the medium in free space, c_0 is the speed of light in a vacuum and n_0 is the linear refractive index of the medium. The units of $\chi^{(3)}$, n_2, and α_2 are m^2/V^2, m^2/W, and m/W, respectively. If described in electrostatic units (esu or cgs), the imaginary and real components of $\chi^{(3)}$ can be expressed as:

$$\chi_r^{(3)} = n_0^2 n_2/0.039;\ \chi_i^{(3)} = \lambda n_0^2\alpha_2/(0.156\pi) \tag{12}$$

where the units of λ, n_2 and α_2 are cm, cm^2/W, and cm/W, respectively. The molecular cubic hyperpolarizability γ can be expressed as:

$$\gamma = \chi^{(3)}/(CF^4N_A) \tag{13}$$

where N_A is Avogadro's constant, C is the number of moles in solution (per cm^3), and F is the local field factor, which is approximated by the Lorentz formula, $F = (n_0^2 + 2)/3$, with n_0 being the linear refractive index of the solvent.

If the sample thickness L is far smaller than the distance between the sample and aperture d, the nonlinear phase shift is small ($\Delta\phi << \pi$), and the laser beam possesses a Gaussian profile, the nonlinear refraction $T_c(x)$ can be approximated as:

$$T_c(x) = 1 - 4x\Delta\phi/[(1 + x^2)(9 + x^2)] \quad (14)$$

where $x = z/z_0$, $z_0 = k\omega_0^2/2$, $k = 2\pi/\lambda$, ω_0 is the beam waist at the focal point, z_0 is the Rayleigh length, λ is the wavelength, and $\Delta\phi$ is the nonlinear phase shift. Now:

$$\Delta\phi = kn_2I_0L_{eff} \quad (15)$$

for I_0 the on-axis intensity at the focus and L_{eff} the effective sample thickness. By fitting experimental $T_c(z)$ data using equation (14), one obtains $\Delta\phi$ and ω_0. Given I_0, λ, L_{eff}, and $\Delta\phi$ are all known, one can then calculate n_2 from $\Delta\phi$ using equation (15).

For a laser beam with a Gaussian profile and a nonlinear absorption process dominated by two-photon absorption, $T_o(x)$ can be approximated as:

$$T_o(x) = (1 - R)^2 e^{-\alpha L} \frac{\ln(1 + q)}{q} \quad (16)$$

where $R = (n_0 - 1)^2/(n_0 + 1)^2$, $q = q_0/(1 + x^2)$, and $q_0 = \alpha_2 I_0 L_{eff}$.

Calculating the nonlinear absorption cross-section from the Z-scan experiment requires fitting the open-aperture and closed-aperture traces with the known values of λ, ω_0, and L_{eff}.

3.2 Indirect methods

The most common indirect method of determining MPA is by nonlinear absorption-induced fluorescence. The nonlinear absorption spectrum of a given MPA-active material can be obtained by measuring the output fluorescence intensity following two-, three-, four- or five-photon excitation. In a typical two-photon excitation setup (**Fig. 3**), ultrashort pulse-length high-power coherent light is passed through the 2PA-active fluorophore. This results in two photons being absorbed simultaneously, and the molecule being excited from the ground state to the excited state. For 2PA, the wavelength of the excitation light source is around twice that of the gap between the ground state and the first excited state of the molecule for dipolar molecules, for which the $S_0 \rightarrow S_1$ transition is allowed for both 1PA and 2PA. With quadrupolar molecules, the $S_0 \rightarrow S_1$ 1PA-allowed transition is two-photon forbidden, and the lowest energy two-photon allowed transition is $S_0 \rightarrow S_2$. The fluorescence emission intensity is proportional to the population of the relevant excited singlet state:

$$I_{fluo} = AI_{pump}^n \quad (17)$$

where I_{fluo} is the fluorescence emission intensity from the MPA process, I_{pump} is the input power energy from the laser, A is the relative conversion efficiency, and n is the number of photons for the MPA process [68,69]. The 2PA spectrum is related to the 2PA cross-section of a molecule and its fluorescence quantum yield, with the latter usually assumed to be equal to that measured under ordinary one-photon excitation. MPEF offers the advantages of high sensitivity, broad wavelength coverage, and speed. However, it cannot be used to measure non-fluorescent chromophores, and unfortunately many strongly MPA-active organic and organometallic compounds show little or no fluorescence [70].

(insert Figure 3 here)

4. MPA-active metal alkynyl complexes

The MPA properties of a wide variety of materials, including organic molecules, polymers, metal-organic frameworks (MOFs), perovskite nanomaterials, carbon-based materials, and inorganic and organometallic complexes have been reported. For the last-mentioned, metal alkynyl complexes have attracted especial interest; the polarizable metal centre and the directly bound alkynyl ligand facilitate high electron mobility, and strongly-allowed metal-to-ligand or ligand-to-metal charge transfer. Furthermore, metal alkynyl complexes offer flexibility in the tuning of the structural and electronic properties of both their organic and inorganic constituents, which is ideal for the design and optimization of novel NLO-efficient materials.

The first examples of 2PA-efficient metal alkynyl complexes were reported in the mid-1990s [71-76], and this area continues to attract interest, with recent advances in ultrashort-pulse high-powered lasers permitting extension to higher-order nonlinear absorption phenomena. In early studies, molecular design rules for efficient quadratic NLO-active materials were developed for small organic molecules, and these were then propagated to the coordination and organometallic complex and macromolecular realms [77-79]. Structure-cubic NLO property correlations have also been established with organic molecules and then applied to organometallics, but limitations remain in our understanding [8,56,70]. Models derived from perturbation theory have been beneficial in cubic NLO-material design of small uniaxial organic molecules, for which the third-order hyperpolarizability can be approximated as:

$$\gamma \approx -\frac{\mu_{ge}^4}{E_{ge}^3} + \frac{\mu_{ge}^2 \mu_{ee'}^2}{E_{ge}^2 E_{ge'}} + \frac{\mu_{ge}^2 (\mu_{ee} - \mu_{gg})^2}{E_{ge}^3} \quad (18)$$

where $\mu_{ee'}$ and μ_{ge} are transition dipole moments, μ_{gg} is the ground-state dipole moment, μ_{ee} is the dipole moment at an excited state, and E_{ge} and $E_{ge'}$ are optical absorption energies. Negative

γ results when the first term is dominant, such as with cyanines and squarylium dyes. With centrosymmetric polyenes, the second term dominates and the third term is zero, and a positive γ results. Polyenes with donor and acceptor groups at the termini exhibit a larger γ than their centrosymmetric parents due to contributions from the third term. Viewed more broadly, this expression suggests that molecules with large, polarizable π-electron structures have potential for strong cubic NLO responses, and this prediction has been used to develop cubic NLO-active molecules of more complex geometries. The extrapolation from 2PA-active molecules to molecules that may exhibit significant higher-order NLO effects is assisted by the general observation that large π-electron delocalization, accompanied by strong intramolecular charge transfer, is expected to afford strong MPA. Molecules with dipolar, quadrupolar, and octupolar ground-state charge distributions have all been found to be NLO-efficient [63,80-82].

4.1 Two-photon absorption at metal alkynyl complexes

Metal alkynyl complexes possess a beneficial structure for NLO effects because the incorporation of the metal atom in the plane of the chromophore π-system and strong coupling via the alkynyl linkage results in good electron delocalization, large polarizabilities, and fast responses [63,83]. The cubic NLO and 2PA properties of metal alkynyl complexes have consequently been the subject of considerable study, affording a number of key structure-property correlations [80,84]. As mentioned above, dipolar, quadrupolar, and octupolar compounds have attracted attention as NLO-active molecules, and this has also been the case with organometallics and, more specifically, metal alkynyl complexes. The discussion that follows organizes the complexes by these broad multipolar charge distributions, with further organization by transition series group. Maximal values that aid structure-property correlations are presented in tables, where available; in the absence of such data, general comments are made in the text.

Recent structure-property studies have focussed on ruthenium and platinum (and to a lesser extent nickel and gold) alkynyl complexes, earlier studies having highlighted the particular strengths of these specific metals. The ruthenium(II) complexes possess 18 valence electrons and can be rendered electron-rich with appropriate phosphine co-ligands. Certain complex classes feature two (different) alkynyl ligands at the axial sites of pseudo-octahedral ruthenium centres, and such building blocks can be rapidly assembled into large π-delocalizable (multi)metallic complexes [85-88]. The limited nickel(II) complexes possess 18 valence electrons and an earth-abundant metal, but the single alkynyl ligand limits structural diversity and the less polarizable 3d metal results in diminished NLO merit. Square planar platinum(II) complexes possess 16 valence electrons, frequently with two *trans*-disposed alkynyl ligands that facilitate formation of π-extended structures, and in some cases readily accessible triplet states that facilitate singlet oxygen generation and display cytotoxicity [89,90]. Linear gold(I)

complexes possess 14 valence electrons and, with one alkynyl ligand only, have less potential in the covalent assembly of large NLO-active π-systems; however, they frequently display increased optical transparency which can facilitate the development of structure-activity relationships, they can assemble into increased dimensionality structures via aurophilic interactions, and they can display biological activity [91-93].

4.1.1 Dipolar metal alkynyl complexes

The ligated metal unit of dipolar metal alkynyl complexes has largely featured as the donor in D-B-A constructions targeting MPA. Earlier studies focussed on tuning the donor strength by varying the co-ligands and thereby modifying the 2PA merit [75]. Recent studies have examined the effect of modifying the bridge linking the metal donor to a fixed acceptor or, conversely, using a ligated metal unit as a key component of a bridge that links organic donors and acceptors.

Studies that were directed at pinpointing the most efficient π-bridge in metal alkynyl complexes possessing a [metal donor]-[alkynyl-attached π-bridge]-[acceptor] composition have focussed on identifying the optimum bridge composition, length and breadth. Homoatomic (carbon-based) bridges such as those comprised of arylenes linked by yne or ene groups have proven to be more efficient than heteroatomic bridges such as those linked by azo or imino groups [75]. Both *p*-phenyleneethynylene (PE)- and *p*-phenylenevinylene (PV)-based bridge lengthening have been systematically studied (Table 1, **Fig. 4**) [80]. The 2PA performance plateaus at a certain length and thereafter can diminish on further lengthening, and so there is an optimum length. For example, increasing the length of the alkynyl ligand (proceeding from **1** to **2** and then **3**, **4** to **7** and then **16**, **4** to **5**, **7** to **8**, and **14** to **15**) results in an increase in 2PA cross-section, while the further increase in bridge length from the di(phenyleneethynylene) to the tri(phenyleneethynylene) may lead to a decrease in $\sigma_{2,max}$.(on proceeding from **5** to **6**, and **8** to **9**). The facile rotation about the C(aryl)-C(ethyne) bonds in these OPEs, and the resultant loss of co-planarity, is assumed to impact deleteriously on MPA merit. Enforcing π-bridge coplanarity with appropriately designed alkynyl ligands has not as yet been systematically explored, although this is anticipated to increase the bridge length at which saturation is seen, and thereby improve the 2PA merit of the system.

(insert Figure 4 here)

Table 1. Linear optical absorption and 2PA data.[a,b]

Complex	λ_{max} (nm) [ε (10^4 M^{-1} cm^{-1})]	σ_2 (GM) (λ_{max} (nm))

1	320 [1.9]	300 ± 100 (650)
2	386 [3.1]	1200 ± 200 (800)
3	413 [3.5]	2100 ± 750 (860)
4	485 [1.6]	550 ± 100 (880)
5	467 [2.7]	3000 ± 450 (1050)
6	380 [3.9]	1700 ± 500 (950)
7	483 [2.5]	850 ± 250 (950)
8	472 [2.8]	2200 ± 700 (950)
9	389 [6.9]	1300 ± 450 (950)
10	482 [1.6]	250 ± 50 (900)
11	471 [2.4]	2300 ± 350 (900)
12	374 [2.1]	1100 ± 150 (900)
13	481 [3.4]	2100 ± 550 (950)
14	499 [1.5]	1500 ± 300 (880)
15	477 [1.3]	1400 ± 350 (1100)
16	464 [2.4]	1100 ± 150 (950)
17	477 [2.8]	1800 ± 500 (950)

[a] Measurements in CH_2Cl_2. [b] Data from Ref. 80.

The importance of the specific location of the metal in the chromophore has also been explored. The data for the isomers **5** and **7** and the isomers **6**, **8**, and **16**, which possess fixed length π-systems with varied metal location, suggest that the optimum location of the ligated ruthenium unit to maximize $\sigma_{2,max}$ in these OPEs is a di(phenyleneethynylene) unit away from the peripheral nitro group.

The effect of bridge "broadening" has been examined with ruthenium, nickel, and gold complexes, on progression from 1,4-phenylene to 1,4-naphthalenylene and 9,10-anthracenylene bridging units (Table 2, **Fig. 5**) [94]. In the ruthenium-containing series, proceeding from **18** to **19** results in an increase in maximal 2PA cross-section, but no further change (within the experimental error margins) is seen on proceeding to the anthracenyl-bridged **20**. There is also no improvement seen progressing from the naphthalenyl- to the anthracenyl-containing bridge in either the nickel or the gold system. The maximal values of the 2PA cross-sections increase on proceeding from the gold complexes to the nickel complexes and then to the ruthenium complexes (proceeding from **23** to **21** and then **19**, and **24** to **22** and then **20**), emphasizing the advantage of proceeding from a 14 valence electron metal centre (gold) to an 18 valence electron metal centre with a 3d less polarizable and less readily oxidized metal (nickel), and then to an 18 valence electron metal centre with a 4d metal that is more polarizable and more readily oxidized (ruthenium).

(insert Figure 5 here)

Table 2. 2PA data.[a, b]

Complex	$\lambda_{2PA,\,max}$ (nm)	σ_2 (GM)
18	740	220 ± 45
	940	390 ± 140
19	660	2800 ± 560
	940	690 ± 130
20	720	1100 ± 150
	880	570 ± 120
21	640	580 ± 95
	920	230 ± 55
22	660	460 ± 75
	920	270 ± 60
23	580	850 ± 130
	820	470 ± 140
24	700	630 ± 75
	920	180 ± 40

[a] Measurements in CH_2Cl_2. [b] Data from Ref. 94.

The MPA behavior of certain platinum alkynyl complexes with diimine ligands has been examined by 2PEF, exciting at 790 nm; the complexes exhibit maximal 2PA values around 600 nm, with generally low molecular cross-sections (10-20 GM) [95]. Within this system, linking the arylalkynyl ligands and constructing triangular metallacycles were found to afford much more 2PA-efficient molecules (Table 3, **Fig. 6**) [96]. The cyclic complex **28** exhibits a 2PA cross-section of 1020 GM at 680 nm while its acyclic analogous **31** has a 2PA cross-section of 40 GM at the same wavelength, indicating that 2PA properties can be dramatically improved via rigidification and planarization of a metallacyclic structure; the more extended and polarizable π-system and more planar conformation of the OPE ligand both contribute to the enlargement of the 2PA cross-sections.

(insert Figure 6 here)

Table 3. Linear optical absorption and 2PA data.[a, b]

Complex	λ_{max} (nm) [ε (10^4 M^{-1} cm^{-1})]	σ_2 (GM) (λ_{max} (nm))
28	338 [12]	1020 (680)
	408 [2.5]	260 (860)
	458 [1.1]	
29	370 [4.4]	120 (740)
	518 [1.4]	670 (1040)

30	315 [5.5]	610 (700)
	350 [4.6]	
	381 [3.7]	
31	321 [6.7]	40 (680)
	344 [6.8]	17 (860)
	414 [0.8]	

[a] Measurements in CH_2Cl_2. [b] Data from Ref. 96.

Platinum-based photosensitizers are promising anticancer agents in photodynamic therapy [97], and this potential application has been a major reason for interest in the 2PA properties of platinum alkynyl complexes. For example, while **32** exhibits a moderate 2PA cross-section (180 GM) within the biological window (600-900 nm), it inhibits tumour growth in mice at a low dose with negligible side effects (**Fig. 7**).

(insert Figure 7 here)

As mentioned above, the one-photon absorption of gold(I) alkynyl complexes often occurs in the UV region, rendering them essentially optically transparent at key measurement wavelengths such as 532 nm [98]. Changing the ancillary ligand in three series of Au(I) fluorenyl benzothiazole complexes (PMe_3, PPh_3, PCy_3) does not drastically affect the 2PA behavior (Table 4, **Fig. 8**). Proceeding from complexes with a directly bound fluorenyl unit to analogues with an ethynylfluorenyl-based ligand results in an unclear outcome; there is a substantial decrease from **33** to **34**, but small increases from **36** to **37** and **39** to **40**. There is also a general improvement in σ_2 on proceeding from monometallic to bimetallic complex, with the exception of the anomalously 2PA-efficient complex **33** [99].

(insert Figure 8 here)

Table 4. Linear optical absorption and 2PA data.[a, b]

Complex	λ_{max} (nm)	σ_2 (GM) (λ_{max} (nm))
33	359	3000 (590)
36	360	210 (590)
39	364	230 (590)
34	366	230 (570)
37	367	410 (590)
40	371	360 (590)
35	383	1440 (600)

38	384	1320 (600)
41	387	1500 (600)

[a] Measurements in aerated toluene. [b] Data from Ref. 99.

4.1.2 Quadrupolar and centrosymmetric metal alkynyl complexes

In contrast to dipolar compounds, centrosymmetric compounds do not exhibit even-order NLO effects, and the selection rules for 2PA-induced transitions differ from those for 1PA transitions in centrosymmetric compounds, so study of the 2PA properties of centrosymmetric compounds is complementary to studies of related dipolar examples. As with dipolar complexes, the focus of research with quadrupolar and centrosymmetric metal alkynyl complexes has been with examples containing PE- or PV-based bridges.

Incorporating multiple PV units in the bridge of ruthenium end-functionalized complexes results in a red-shift in one-photon absorption (proceeding from **42** (2PV units) to **43** (4PV units), and then **44** (8 PV units): Table 5, **Fig. 9**). The increase in maximal 2PA cross-section proceeding from **42** to **43** is greater than the increase proceeding from **43** to **44**, suggesting a saturation in this response parameter on OPV lengthening [100].

(insert Figure 9 here)

Table 5. Linear optical absorption and 2PA data.[a, b]

Complex	λ_{max} (nm) [ε (10^4 M^{-1} cm^{-1})]	σ_2 (GM) (λ_{max} (nm))
42	463 [7.7]	2 650 (800)
43	476 [11.8]	10 000 (725)
44	484 [18.0]	12 500 (725)

[a] Measurements in CH_2Cl_2. [b] Data from Ref. 100.

Complexes **45** and **46** exhibit the lowest σ_2 values of the tetraruthenium complexes **45**, **46-48**, and **49-50**, consistent with their smaller molecular size and lack of polarizing substituents (Table 6, **Fig. 10**). Introduction of electron-donating or -withdrawing substituents at the periphery of **45**, in proceeding to **47** and **48**, significantly improves nonlinear absorption merit. The data also suggest that the electron-withdrawing nitro substituent is more effective in increasing σ_2 than the electron-donating diethylamino substituent [101].

Table 6. Linear optical absorption and 2PA data.[a, b]

Complex	λ_{max} (nm)	σ_2 (GM)

	[ε (10^4 M^{-1} cm^{-1})]	(λ_{max} (nm))
45	335 [13.9]	0 ± 7 (920)
46	335 [14.1] (THF)	40 ± 40 (840)
47	342 [12.2], 481 [8.1]	1400 ± 300 (880)
48	342 [16.2]	900 ± 300 (880)
49	367 [18.8]	480 ± 40 (920)
50	462 [4.2]	5500 ± 1500 (880)

[a] Measurements in CH_2Cl_2 unless otherwise specified. [b] Data from Ref. 101.

(insert Figure 10 here)

The cruciform complexes **52** and **53** display no variation in 2PA cross-section on modifying their peripheral groups, π-system expansion (proceeding from **51** to **52** and **53**) being the key structural change to improve 2PA (Table 7, **Fig. 11**) [102,103]. An increasingly electronegative periphery (proceeding from **56** to **55** and then **54**) increases the maximal 2PA value in the substituted porphyrins **54**-**56**.

(insert Figure 11 here)

Table 7. 2PA data.[a]

Complex	σ_2 (GM)	Ref.
51	2090 ± 880 @ 750 nm	[102]
52	4020 ± 1640 @ 750 nm	[102]
53	4020 ± 1640 @ 750 nm	[102]
54	6000 ± 300 @ 770 nm	[103]
55	4800 ± 500 @ 710 nm	[103]
56	4200 ± 500 @ 710 nm	[103]

[a] Measurements in CH_2Cl_2.

Systematic studies of quasi-centrosymmetric platinum alkynyl complexes with phenylethynyl or (9,9-diethyl-7-(phenyl)ethynyl-9*H*-fluoren-2-yl)ethynyl π-bridges have explored alkynyl ligand lengthening, electronic effects, conformation and non-alkynyl ligand influence on 2PA properties (Table 8, **Fig. 12**) [104-107]. Complexes with simple phenylethynyl-derived ligands (structures **a**) display a general decrease in 2PA cross-section following the trend: compounds with electron-withdrawing groups > compounds with electron-donating groups > compounds with electro-neutral groups. The *trans*-[Pt(C≡C-1,4-$C_6H_4X)_2(PBu_3)_2$] complexes (structures **a**) exhibit at least a doubling in 2PA cross-section (and in many cases frequently greater increases) in proceeding to their fluorenyl-bridged analogues (structures **b**).

The OPE-based complexes **79** and **80** display the same trend on π-bridge lengthening as their ruthenium alkynyl counterparts; the 2PA peaks exhibit a red-shift and the cross-sections increase upon π-ligand lengthening [106,107].

(insert Figure 12 here)

Table 8. 2PA data.[a]

Complex	$\lambda_{2PA,max}$ (nm)	σ_2 (GM)	Ref.
57	682	15	[104]
58	782	93	[105]
59	668	10	[104]
60	774	57	[105]
61	712	16	[104]
62	810	33	[105]
63	672	1	[104]
64	772	73	[105]
65	670	1	[104]
66	774	61	[105]
67	672	1	[104]
68	774	92	[105]
69	668	1	[104]
70	772	53	[105]
71	752	120	[104]
72	826	270	[105]
73	684	2	[104]
74	792	120	[105]
75	702	8	[104]
76	814	190	[105]
77	774	120	[104]
78	862	700	[105]
79	570	320 (CH_2Cl_2 solvent)	[106]
	710	45 (CH_2Cl_2 solvent)	
80	610	680 (CH_2Cl_2 solvent)	[107]
	760	120 (CH_2Cl_2 solvent)	

[a] Measurements in THF unless otherwise noted.

For the series of compounds **81**-**88**, effective nonlinear absorption coefficients increase on metalation (proceeding from **81** to **82**), proceeding from quadrupolar **82** to dipolar **83**, replacement of electron-withdrawing peripheral groups with electron-donating (proceeding

from **83** to **82**), and increasing metalation (proceeding from **82** to **87** or **84** to **85**), while bridge broadening (proceeding from **85** to **86** or **87** to **88**) leads to a reduction in this metric (Table 9, **Fig. 13**) [108].

(insert Figure 13 here)

Table 9. Effective nonlinear absorption coefficients.[a, b]

Complex	β (cm/GM)
81	9.03
82	46.5
83	95.3
84	21.3
85	100.1
86	45.74
87	248.1
88	110.8

[a] Measurements in DMF. [b] Data from Ref. 108.

The effect on nonlinear absorption properties of the progression from dipolar to centrosymmetric platinum alkynyl complex has been explored (**Fig. 14**) [109]. The $S_0 \rightarrow S_1$ transition that is allowed for dipolar complexes is forbidden for centrosymmetric complexes, the lowest energy intense 2PA transition being $S_0 \rightarrow S_2$ (for non-centrosymmetric chromophores (e.g. dipolar examples), the 2PA spectrum is degenerate with the one-photon absorption) [110]. Consistent with expectations, the *trans*-ligated (centrosymmetric) complexes **91** and **93** show 2PA peaks at ca. 640-650 nm (σ_2 up to 1000 GM), red-shifted to 750 nm progressing to **89** due to the electron-withdrawing benzothiazole ring. The (dipolar) *cis*-complexes **92** and **94** exhibit the expected, red-shifted maxima at ca. 715-755 nm which increase in intensity on proceeding to the benzothiazole-containing **90**.

(insert Figure 14 here)

Platinum(II) complexes with triphenylamine-functionalized OPV-based alkynyl ligands afford strong 2PA performance over a broad spectral window [111]. The 2PA data increase with lengthening of the OPV segment (proceeding from **96** to **97** and then **98**, from **99** to **100** and then to **101**, and from **104** to **105**). The peak 2PA values increase approximately two-fold proceeding from the organic chromophores **99** and **100** to the corresponding Pt-complexes **96**

and **97**, and more than two-fold from **101** to **98**. Complex **98** and **103** both exhibit exceptionally large 2PA cross-sections (greater than 10 000 GM) at short wavelengths.

(insert Figure 15 here)

trans-Ligated platinum bis(alkynyl) complexes with *N*-heterocyclic carbene ligands have been compared to their tri(*n*-butyl)phosphine analogues, to assess the effect of ligand variation on their 2PA properties (**Fig. 16**) [112]. The σ_2 values increase as **106** < **107** < **108** ≈ **91**, consistent with increasing polarization (π-system lengthening and installation of donor/acceptor substituents on the periphery) and incorporation of peripheral donor rather than acceptor groups enhancing 2PA cross-section, while the co-ligand replacement has minimal impact.

(insert Figure 16 here)

2PA cross-sections of donor-acceptor-donor structures increase on proceeding from organic diyne to derivative gold(I) alkynyl complex and then platinum(II) alkynyl complex (**Fig. 17**) [113]. Data for the gold alkynyls are modest (ca. 150 GM), while the platinum complexes display stronger activity in the first biological window, exhibiting greater σ_2 in the 800-900 nm region (200-600 GM), and with values approaching 1000 GM at wavelengths below 800 nm.

(insert Figure 17 here)

Nonlinear absorption studies of 1,4-{$(Cy_3P)Au(C{\equiv}C)\}_2C_6H_4$ (**114**) and its 6-fold symmetric analogue {$(Cy_3P)Au(C{\equiv}C\text{-}1,4\text{-}C_6H_4C{\equiv}C)\}_6C_6$ (**115**) [114] reveal a dramatic increase in 2PA cross-section at ca. 600 nm proceeding from **114** (18 GM) to **115** (9000 GM) that persists after scaling the data to correct for relative molecular weights (σ_2/M: 0.017 and 2.4, respectively) or the number of PE units in the bridge (**Fig. 18**).

(insert Figure 18 here)

The 2PA properties of transition metal σ-alkynyl complex-based polymers have also been explored [115]. Inserting transition metal elements into the main chain of polymers may combine the advantages of both transition metals and polymers to improve overall NLO performance. The NLO properties of gold(I) and platinum(II) alkynyl complexes and oligomers with thienyl-carbazole structure were explored to test this idea as well as further

examine the impact of metal variation (**Fig. 19**) [116]. **116**, **117** and **118** show similar nonlinear absorptive behaviour, with low 2PA cross-sections in the $S_0 \rightarrow S_1$ region (σ_2 ~ 10-100 GM at 700-800 nm). The cross-sections increase rapidly on proceeding to shorter wavelengths, reaching values of ca. 800-1000 GM at 550 nm.

(insert Figure 19 here)

Platinum alkynyl polymers **120** and **121** with different substituent groups (electron donor, O-*n*-Bu; electron acceptor, NO_2) are derived from **119** (**Fig. 20**); their 2PA cross-sections at 795 nm are relatively invariant to the nature of this polarizing substituent (**120**: 53-89 GM; **121**: 45-70 GM) [117].

(insert Figure 20 here)

The nonlinear properties of platinum alkynyl-based polymers lacking continuous backbone π-systems have also been explored, in the pursuit of optical limiting materials [118]. Poly(arylene ether)-based **122** and **123** exhibit good optical transparency and large nonlinear absorption coefficients at 532 nm (**122**: 0.59 cm/GW, **123**: 2.42 cm/GW) (**Fig. 21**).

(insert Figure 21 here)

4.1.3 Octupolar metal alkynyl complexes and dendrimers

The progression from linear ruthenium alkynyl complexes to analogous stars [102,119] is an efficient strategy to achieve excellent nonlinear absorption in the second biological transmission window (1000-1350 nm). Increasing the number of PE units in the arms of the star results in a noticeable increase in 2PA cross-section (proceeding from **124** to **127**, **130**, **131**, and **132**: Table 10, **Fig. 22**). The effect of peripheral ligand modification has been investigated as well, revealing that replacing the phenyalkynyl ligands with *p*-nitrophenylalkynyl ligands generally increases σ_2 (proceeding from **125** to **126**, or from **128** to **129**). The results from replacing the PE linkage with PV linkage are unclear: proceeding from **124** to **133** has little effect on σ_2, but proceeding from **125** to **134** results in a significant increase in the 2PA cross-section.

Table 10. Linear optical absorption and cubic NLO data.[a]

Complex	λ_{max} (nm) [ε (10^4 $M^{-1}cm^{-1}$)]	σ_2 (GM) (λ_{max} (nm))	Ref.
124	413 [9.9]	1500 ± 140 (680) 1050 ± 400 (845)	[119]
125	412 [11.6]	1490 ± 200 (650) 370 ± 80 (810)	[119]
126	403 [11.2] 459 [8.9]	2500 ± 1000 (670) 1100 ± 400 (800-950)	[119]
127	424 [13.5]	9500 ± 1800 (650) 6000 ± 1600 (875)	[119]
128	422 [12.6]	3200 ± 1400 (900)	[119]
129	418 [11.6] 459 [8.8]	6000 ± 1200 (875)	[119]
130	416 [13.0]	6000 ± 1200 (875)	[119]
131	420 [14.8]	7600 ± 1300 (900)	[119]
132	412 [19.6]	5500 ± 1500 (880)	[119]
133	426 [8.7]	1000 ± 200 (800) (THF solvent)	[102]
134	421 [13.0]	2100 ± 500 (800) (THF solvent)	[102]

[a] Measurements in CH_2Cl_2 unless otherwise noted.

(insert Figure 22 here)

The cubic NLO properties of octupolar platinum alkynyl complexes have also been studied (**Fig. 23**) [11,120]. The 2PA cross-sections of 1,3,5-triazine-cored complexes (with an electron-withdrawing core) increase with increasing electron-donating ability of the arylalkynyl substituent in **135**-**137**. Among the triphenylamine-centred complexes **138**-**140** (with electron-donating cores), the largest 2PA value is found with complex **140** which possesses the most strongly electron-withdrawing substituent on the arylalkynyl ligand. Pt(II) alkynyl complexes with a 1,3,5-triazine core and 3,4,5-tris(dodecyloxy)benzamide terminal units have also been explored [11]; the 2PA cross-section of complex **141** (707 GM at 532 nm in toluene) and its good gelation properties are consistent with potential as an optical limiting gelation material.

(insert Figure 23 here)

Proceeding from octupolar stars to hyper-branched dendrimers is a logical progression in the quest for efficient 2PA materials. Ruthenium alkynyl dendrimers have been shown to possess significant third-order NLO properties, greater than the sum of the linear components, and outperforming the building blocks when scaling for number of π-electrons or molecular weight

(**Fig. 24**) [87,88,121-124]. These two performance-scaling procedures have been employed to compare both similar and disparate molecules. Scaling by the appropriate power of the number of "effective" electrons is a rigorous procedure introduced by Kuzyk with small organic molecules [125]. Its application to metal alkynyl complexes has necessitated certain assumptions regarding the contribution of the metal centre when located between two *trans*-disposed π-delocalizable ligands. Scaling by molecular weight is a simpler and more widely employed approach to compare molecular NLO performance, but the presence of high-mass-unit ligated metal centres can result in unfavourable comparisons to related purely organic molecules. Scaling by molecular volume and cost of production have also been employed, but their difficulty in implementation has restricted the take-up of these procedures [126].

Dendrimers with both OPE and OPV building blocks have been reported, their 2PA cross-section values being collected in Table 11. There is more than an order of magnitude increase in σ_2 on proceeding from the first-generation to the second-generation and then to the third-generation dendrimer [124]. These ruthenium alkynyl dendrimers exhibit a cubic NLO dendritic effect, i.e. a nonlinear increase in nonlinearity with increase in dendrimer generation.

(insert Figure 24 here)

Table 11. Linear optical absorption and 2PA data.[a]

Complex	λ_{max} (nm) [ε (10^4 $M^{-1}cm^{-1}$)]	σ_2 (GM) (λ_{max} (nm))	Ref.
150	346 [222]	111 500 (700)	[124]
	424 [81]	50 600 (900)	
149	340 [206]	113 200 (725)	[124]
	418 [106]	45 900 (900)	
148	343 [119]	42 450 (750)	[124]
	421 [52]	16 000 (875)	
147	343 [118]	43 600 (700)	[124]
	415 [49]	20 000 (900)	
143	340 [43]	13 700 (725)	[87, 124]
	427 [19]	8800 (900)	
146	340 [96]	34 700 (750)	[87, 124]
	409 [46]	18 000 (900)	
142	343 [38]	14 000 (725)	[87, 124]
	412 [18]	6300 (875)	
144	333 [45]	4400 (760)	[88]
	424 [18]	-	
145	311 [40]	17 000 (780)	[88]
	390 [59]	-	

[a] Measurements in CH_2Cl_2.

4.2 Higher-order multiphoton absorption at metal alkynyl complexes

Higher-order multiphoton absorption properties such as three-photon absorption (3PA), four-photon absorption (4PA) and five-photon absorption (5PA) are of rapidly increasing interest because of their potential advantages compared to 2PA. MPA is more sensitive to light intensity, permitting even greater spatial control. Because the excitation is shifted to longer wavelengths with MPA (e.g. into the biological and telecom windows), MPA may have technological utility in various areas. Studies of the MPA efficiency of diverse materials are therefore of considerable interest [39,78,127], but molecular structure-property studies are sparse.

Several systematic studies exploring higher-order MPA properties of metal alkynyl complexes have been reported [88,100,119]. The first such report [128] disclosed the nonlinear absorption properties of dendrimer **151**, evaluated from Z-scan over the spectral range 625-1500 nm with fs pulses to minimize contributions from excited-state absorption (ESA). The maximal value for σ_3 (1500×10^{-80} cm^6 s^2 $photon^{-2}$) was a record for a molecule, and highlighted the potential of alkynyl complexes in MPA.

(insert Figure 25 here)

The organoruthenium stars [100,119] display 3PA at the high-energy end of the telecom window and this increases with arm lengthening, proceeding from **124** to **127**, and then to **130**, **131**, and **132**. The data approach a saturation point, indicating that further OPE lengthening is unlikely to significantly improve MPA merit. The same trend appears with centrosymmetric OPV-based ruthenium alkynyl complexes, for which nonlinear absorption studies have examined bridge lengthening from 1 PV unit up to 8 PV units (proceeding from **42** to **43** to **44**); the initial arm lengthening (proceeding from 1 PV unit to 2 PV units) results in a significant increase in the maximal 3PA value, but further increase in the number of PV units affords only a minor increase in σ_3. Investigation of the effect of peripheral ligand modification reveals a significant increase in σ_3 value for the *p*-nitrophenylalkynyl-containing complexes compared with the chlorido-/phenylalkynyl-ligated analogues (comparing **124** and **125** to **126**, or **127** and **128** to **129**). Complex **129** shows a larger σ_3 value than any other star complex, and also displays measurable 4PA activity, revealing a modest σ_4 value.

Table 12. Linear optical absorption and MPA data.[a]

Complex	λ_{max} (nm) [ε (10^4 $M^{-1}cm^{-1}$)]	σ_3 [b] (λ_{max} (nm))	σ_4 [c] (λ_{max} (nm))	Ref.

124	413 [9.9]	190 ± 50 (1290)	-	[119]
125	412 [11.6]	100 ± 20 (1240)	-	[119]
126	403 [11.2] 459 [8.9]	740 ± 130 (1290)	-	[119]
127	424 [13.5]	1800 ± 300 (1200)	-	[119]
128	422 [12.6]	2300 ± 600 (1200)	-	[119]
129	418 [11.6] 459 [8.8]	5000 ± 800 (1200)	180 ± 50 (1750)	
130	416 [13.0]	1800 ± 300 (1200)	-	[119]
131	420 [14.8]	3200 ± 500 (1250)	-	[119]
132	412 [19.6]	3300 ± 400 (1250)	-	[119]
42	463 [7.7]	3500 (1100)	-	[100]
43	476 [11.8]	11 000 (1100)	-	[100]
44	484 [18.0]	15 500 (1100)	-	[100]

[a] Measurements in CH_2Cl_2. [b] 10^{-80} cm^6 s^2 $photon^{-2}$. [c] 10^{-110} cm^8 s^3 $photon^{-3}$.

Ruthenium-containing dendrimers exhibit exceptional MPA activities [87,88,128]. As shown in Table 13, increasing the length of the π-bridge directly attached to the dendrimer core (proceeding from **142** to **143** or **146** to **147**) generally results in an increase in nonlinear absorption parameters, while introducing solubilizing alkyl groups (proceeding from **147** to **148** or **149** to **150**) has a very subtle impact on MPA cross-sections. Significant increases in MPA cross-sections are seen on increase in dendrimer generation, on proceeding from first-generation dendrimers **142** and **143** to second-generation dendrimers **146** and **147**-**148**, and then to third-generation dendrimers **149**-**150**. Amongst the first-generation dendrimers, **145** possesses the largest 3PA cross-section value, and comparison of the MPA data of **144** and **145** clearly highlights the importance of metalation at each dendritic generation level to the resultant MPA properties.

Table 13. 3PA, 4PA and 5PA cross-section maxima.[a]

Complex	σ_3 [c] (λ_{max})[b]	σ_4 [d] (λ_{max})[b]	σ_5 [e] (λ_{max})[b]	Ref.
150	23 200 (1250)	7300 (1650)	500 (2050)	[124]
149	22 200 (1200)	5850 (1650)	350 (2100)	[124]
148	15 000 (1250)	3700 (1650)	170 (2100)	[124]
147	13 750 (1250)	2950 (1650)	100 (2160)	[124]
146	4800 (1200)	1200 (1650)	-	[124]

143	7950 (1250)	2700 (1650)	-	[124]
142	2500 (1250)	900 (1650)	-	[124]
145	10 000 (1200)	2100 (1600)	-	[88]
144	3500 (1100)	-	-	[88]

[a] Measurements in CH_2Cl_2. [b] nm. [c] 10^{-80} cm^6 s^2 $photon^{-2}$. [d] 10^{-110} cm^8 s^3 $photon^{-3}$. [e] 10^{-140} cm^{10} s^4 $photon^{-4}$.

(insert Figure 26 here)

Figure 26 displays a typical MPA study (that of **149**) and highlights the need for tuneable wavelength lasers (as the phenomena are wavelength-dependent). The maximal values of the nPA are usually seen at close to the corresponding multiple of the linear absorption spectrum, and so this is often supplied as an overlay in the NLA spectrum to provide an eye guide. Figure 26 also emphasizes the need for careful intensity-dependence measurements, to discriminate between nPA and (n+1)PA effects, and hints at the time-intensive nature of such studies (the laser is tuned to each wavelength individually, data are collected, and the laser is then tuned to the subsequent wavelength).

5. Conclusion and perspectives

The increasing availability of high-power, ultrashort pulse, wavelength-tunable laser systems is making the systematic study of molecular MPA properties a realistic goal. Studies over the previous decade have demonstrated that metal alkynyl complexes can be engineered to possess very large MPA properties, frequently outperforming the best organics. Although comparing disparate materials is challenging, the procedures explored thus far (scaling by molecular volume, cost, molecular weight-, and the number of "effective" electrons) all afford results consistent with metal alkynyl complexes trumping purely organic compounds.

Systematic studies of metal alkynyl complexes have explored the effect of varying the co-ligands, alkynyl ligands, conformation, the nature of the metal, and the multipolar charge distribution in the ground state, and these studies have expanded to include metal alkynyl-based polymers and dendrimers. Exceptionally large (world-record) values of MPA cross-sections have been demonstrated with certain examples, highlighting the considerable potential of metal alkynyl complexes. The studies thus far have begun to signpost the metal alkynyl complex composition considerations to maximize MPA merit. The design of robust and stable materials with strong MPA response applicable to the construction of smart devices remains a goal for researchers and a challenge for future work.

Conflicts of interest

The authors declare that they have no known competing financial interests or personal relationships that could have appeared to influence the work reported in this paper.

Acknowledgements

L.Z. thanks the China Scholarship Council and the Australian National University for an ANU-CSC Postgraduate Scholarship. M.G.H. thanks the Australian Research Council for continuing support (current grant: DP220100111).

References

[1] G. New, Introduction to Nonlinear Optics, Cambridge University Press, Cambridge, 2011.

[2] E. Garmire, Nonlinear optics in daily life, Opt. Express, 21 (2013) 30532-30544. https://doi.org/10.1364/OE.21.030532.

[3] H.A. Abdeldayem, D.O. Frazier, in: Nonlinear Optics and Applications, H.A. Abdeldayem, D.O. Frazier (Eds.), NASA Goddard Space Flight Center; Greenbelt, MD, United States, 2007.

[4] P. Weinberger, John Kerr and his effects found in 1877 and 1878, Philos. Mag. Lett., 88 (2008) 897-907. https://doi.org/10.1080/09500830802526604.

[5] M. Moreno, in: Kerr Effect, http://www.ifsc.usp.br/~strontium/Teaching/Material2018-1%20SFI5708%20Eletromagnetismo/Monografia%20-%20Michelle%20-%20Kerr.pdf, 2018 (accessed 17 August 2022).

[6] Y. B. Band, Light and Matter: Electromagnetism, Optics, Spectroscopy and Lasers, Wiley, 2006, p 656. ISBN: 978-0-471-89931-0.

[7] J. Hecht, A short history of laser development, Appl. Opt., 49 (2010) 99-122. https://doi.org/10.1364/AO.49.000F99.

[8] P.A. Franken, A.E. Hill, C.W. Peters, G. Weinreich, Generation of Optical Harmonics, Phys. Rev. Lett., 7 (1961) 118-119. https://doi.org/10.1103/PhysRevLett.7.118.

[9] S. Pascal, Q. Bellier, S. David, P.-A. Bouit, S.-H. Chi, N.S. Makarov, B. Le Guennic, S. Chibani, G. Berginc, P. Feneyrou, D. Jacquemin, J.W. Perry, O. Maury, C. Andraud, Unraveling the Two-Photon and Excited-State Absorptions of Aza-BODIPY Dyes for Optical Power Limiting in the SWIR Band, J. Phys. Chem. C, 123 (2019) 23661-23673. https://doi.org/10.1021/acs.jpcc.9b08376.

[10] W. Feng, K. Liu, J. Zang, G. Wang, R. Miao, L. Ding, T. Liu, J. Kong, Y. Fang, Flexible and Transparent Oligothiophene-o-Carborane-Containing Hybrid Films for Nonlinear Optical

Limiting Based on Efficient Two-Photon Absorption, ACS Appl. Mater. Interfaces, 13 (2021) 28985-28995. https://doi.org/10.1021/acsami.1c07835.

[11] H. Su, S. Zhu, M. Qu, R. Liu, G. Song, H. Zhu, 1,3,5-Triazine-Based Pt(II) Metallogel Material: Synthesis, Photophysical Properties, and Optical Power-Limiting Performance, J. Phys. Chem. C, 123 (2019) 15685-15692. https://doi.org/10.1021/acs.jpcc.9b02168.

[12] H. Lundén, C. Lopes, M. Lindgren, A. Liotta, D. Chateau, F. Lerouge, F. Chaput, A. Désert, S. Parola, Efficient reverse saturable absorption of sol-gel hybrid plasmonic glasses, Opt. Mater., 69 (2017) 134-140. https://doi.org/10.1016/j.optmat.2017.04.024.

[13] S. Pascal, S. David, C. Andraud, O. Maury, Near-infrared dyes for two-photon absorption in the short-wavelength infrared: strategies towards optical power limiting, Chem. Soc. Rev., 50 (2021) 6613-6658. https://doi.org/10.1039/D0CS01221A.

[14] L.W. Tutt, T.F. Boggess, A review of optical limiting mechanisms and devices using organics, fullerenes, semiconductors and other materials, Prog. Quantum Electron., 17 (1993) 299-338. http://dx.doi.org/10.1016/0079-6727(93)90004-S.

[15] N. Liaros, P. Aloukos, A. Kolokithas-Ntoukas, A. Bakandritsos, T. Szabo, R. Zboril, S. Couris, Nonlinear Optical Properties and Broadband Optical Power Limiting Action of Graphene Oxide Colloids, J. Phys. Chem. C, 117 (2013) 6842-6850. https://doi.org/10.1021/jp400559q.

[16] N. Venkatram, D.N. Rao, M.A. Akundi, Nonlinear absorption, scattering and optical limiting studies of CdS nanoparticles, Opt. Express, 13 (2005) 867-872. https://doi.org/10.1364/OPEX.13.000867.

[17] H. Pan, W. Chen, Y.P. Feng, W. Ji, J. Lin, Optical limiting properties of metal nanowires, Appl. Phys. Lett., 88 (2006) 223106. https://doi.org/10.1063/1.2208549.

[18] A.M. Weiner, Ultrafast optical pulse shaping: A tutorial review, Optics Commun., 284 (2011) 3669-3692. https://doi.org/10.1016/j.optcom.2011.03.084.

[19] C. Manzoni, O.D. Mücke, G. Cirmi, S. Fang, J. Moses, S.-W. Huang, K.-H. Hong, G. Cerullo, F.X. Kärtner, Coherent pulse synthesis: towards sub-cycle optical waveforms, Laser Photon. Rev., 9 (2015) 129-171. https://doi.org/10.1002/lpor.201400181.

[20] A.J. DeMaria, D.A. Stetser, H. Heynau, Self Mode-Locking of Lasers with Saturable Absorbers, Appl. Phys. Lett, 8 (1966) 174-176. https://doi.org/10.1063/1.1754541.

[21] U. Keller, Recent developments in compact ultrafast lasers, Nature, 424 (2003) 831-838. https://doi.org/10.1038/nature01938.

[22] T. Brabec, F. Krausz, Intense few-cycle laser fields: Frontiers of nonlinear optics, Rev. Modern Phys., 72 (2000) 545-591. https://doi.org/10.1103/RevModPhys.72.545.

[23] G. Banfi, V. Degiorgio, D. Ricard, Nonlinear optical properties of semiconductor nanocrystals, Adv. Phys., 47 (1998) 447-510. https://doi.org/10.1080/000187398243537.

[24] K. Tanaka, Optical nonlinearity in photonic glasses, J. Mater. Sci.: Mater. Electron., 16 (2005) 633-643. https://doi.org/10.1007/s10854-005-3738-6.

[25] W. Chu, Y. Tan, P. Wang, J. Xu, W. Li, J. Qi, Y. Cheng, Centimeter-Height 3D Printing with Femtosecond Laser Two-Photon Polymerization, Adv. Mater. Technol., 3 (2018) 1700396. https://doi.org/10.1002/admt.201700396.

[26] H. Kita, R. Yamakado, R. Fukuuchi, T. Konishi, K. Kamada, Y. Haketa, H. Maeda, Switching of Two-Photon Optical Properties by Anion Binding of Pyrrole-Based Boron Diketonates through Conformation Change, Chem. Eur. J., 26 (2020) 3404-3410. https://doi.org/10.1002/chem.201905467.

[27] P.-K. Chow, G. Cheng, G.S.M. Tong, W.-P. To, W.-L. Kwong, K.-H. Low, C.-C. Kwok, C. Ma, C.-M. Che, Luminescent Pincer Platinum(II) Complexes with Emission Quantum Yields up to Almost Unity: Photophysics, Photoreductive C≡C Bond Formation, and Materials Applications, Angew. Chem. Int. Ed., 54 (2015) 2084-2089. https://doi.org/10.1002/anie.201408940.

[28] C. Jin, F. Liang, J. Wang, L. Wang, J. Liu, X. Liao, T.W. Rees, B. Yuan, H. Wang, Y. Shen, Z. Pei, L. Ji, H. Chao, Rational Design of Cyclometalated Iridium(III) Complexes for Three-Photon Phosphorescence Bioimaging, Angew. Chem. Int. Ed., 59 (2020) 15987-15991. https://doi.org/10.1002/anie.202006964.

[29] H. Cao, L. Wang, Y. Yang, J. Li, Y. Qi, Y. Li, Y. Li, H. Wang, J. Li, An Assembled Nanocomplex for Improving both Therapeutic Efficiency and Treatment Depth in Photodynamic Therapy, Angew. Chem. Int. Ed., 57 (2018) 7759-7763. https://doi.org/10.1002/anie.201802497.

[30] Pragti, B.K. Kundu, S.N. Upadhyay, N. Sinha, R. Ganguly, I. Grabchev, S. Pakhira, S. Mukhopadhyay, Pyrene-based fluorescent Ru(II)-arene complexes for significant biological applications: catalytic potential, DNA/protein binding, two photon cell imaging and in vitro cytotoxicity, Dalton Trans, 51 (2022) 3937-3953. https://doi.org/10.1039/D1DT04093F.

[31] H. Sund, Y.-Y. Liao, C. Andraud, A. Duperray, A. Grichine, B. Le Guennic, F. Riobé, H. Takalo, O. Maury, Polyanionic Polydentate Europium Complexes as Ultrabright One- or Two-photon Bioprobes, ChemPhysChem, 19 (2018) 3318-3324. https://doi.org/10.1002/cphc.201800557.

[32] C. Mauriello Jimenez, D. Aggad, J.G. Croissant, K. Tresfield, D. Laurencin, D. Berthomieu, N. Cubedo, M. Rossel, S. Alsaiari, D.H. Anjum, R. Sougrat, M.A. Roldan-Gutierrez, S. Richeter, E. Oliviero, L. Raehm, C. Charnay, X. Cattoën, S. Clément, M. Wong, C. Man, M. Maynadier, V. Chaleix, V. Sol, M. Garcia, M. Gary-Bobo, N.M. Khashab, N. Bettache, J.-O. Durand, Porous Porphyrin-Based Organosilica Nanoparticles for NIR Two-Photon Photodynamic Therapy and Gene Delivery in Zebrafish, Adv. Funct. Mater., 28 (2018) 1800235. https://doi.org/10.1002/adfm.201800235.

[33] K. Liu, X. Kong, Y. Ma, W. Lin, Rational Design of a Robust Fluorescent Probe for the Detection of Endogenous Carbon Monoxide in Living Zebrafish Embryos and Mouse Tissue, Angew. Chem. Int. Ed., 56 (2017) 13489-13492. https://doi.org/10.1002/anie.201707518.

[34] L. Zhou, Q. Wang, Y. Tan, M.J. Lang, H. Sun, X. Liu, Rational Development of Near-Infrared Fluorophores with Large Stokes Shifts, Bright One-Photon, and Two-Photon Emissions for Bioimaging and Biosensing Applications, Chem. Eur. J., 23 (2017) 8736-8740. https://doi.org/10.1002/chem.201701365.

[35] B. Gu, W. Wu, G. Xu, G. Feng, F. Yin, P.H.J. Chong, J. Qu, K.-T. Yong, B. Liu, Precise Two-Photon Photodynamic Therapy using an Efficient Photosensitizer with Aggregation-Induced Emission Characteristics, Adv. Mater., 29 (2017) 1701076. https://doi.org/10.1002/adma.201701076.

[36] C. Ouyang, Y. Li, T.W. Rees, X. Liao, J. Jia, Y. Chen, X. Zhang, L. Ji, H. Chao,

Supramolecular Assembly of An Organoplatinum(II) Complex with Ratiometric Dual Emission for Two-Photon Bioimaging, Angew. Chem. Int. Ed., 60 (2021) 4150-4157. https://doi.org/10.1002/anie.202014043.

[37] B. Ma, H. Xu, W. Zhuang, Y. Wang, G. Li, Y. Wang, ROS Responsive Nanoplatform with Two-Photon AIE Imaging for Atherosclerosis Diagnosis and "Two-Pronged" Therapy, Small, 16 (2020) 2003253. https://doi.org/10.1002/smll.202003253.

[38] P. Wang, Y.-L. Xia, L.-W. Zou, X.-K. Qian, T.-Y. Dou, Q. Jin, S.-Y. Li, Y. Yu, D.-D. Wang, Q. Luo, G.-B. Ge, L. Yang, An Optimized Two-Photon Fluorescent Probe for Biological Sensing and Imaging of Catechol-O-Methyltransferase, Chem. Eur. J., 23 (2017) 10800-10807. https://doi.org/10.1002/chem.201701384.

[39] Y. Jiang, K.F. Li, K. Gao, H. Lin, H.L. Tam, Y.Y. Liu, Y. Shu, K.L. Wong, W.Y. Lai, K.W. Cheah, W. Huang, Frequency-Upconverted Stimulated Emission by Up to Six-Photon Excitation from Highly Extended Spiro-Fused Ladder-Type Oligo(p-phenylene)s, Angew. Chem. Int. Ed. Engl., 60 (2021) 10007-10015. https://doi.org/10.1002/anie.202100542.

[40] G. Han, G. Li, J. Huang, C. Han, C. Turro, Y. Sun, Two-photon-absorbing ruthenium complexes enable near infrared light-driven photocatalysis, Nat. Commun., 13 (2022) 2288. https://doi.org/10.1038/s41467-022-29981-3.

[41] C.B. de Araújo, A.S.L. Gomes, G. Boudebs, Techniques for nonlinear optical characterization of materials: a review, Rep. Prog. Phys., 79 (2016) 036401. https://doi.org/10.1088/0034-4885/79/3/036401.

[42] N. Liaros, J.T. Fourkas, The Characterization of Absorptive Nonlinearities, Laser Photon. Rev., 11 (2017) 1700106. https://doi.org/10.1002/lpor.201700106.

[43] G.S. He, A.T. Yeates, P.N. Prasad, K.D. Belfield, F. Kajzar, C.M. Lawson, Three-photon absorbing materials: characterization and applications, Proc. SPIE, 5211 (2003) 1. https://doi.org/10.1117/12.508092.

[44] B. Gu, J. Wang, J. Chen, Y.-X. Fan, J. Ding, H.-T. Wang, Z-scan theory for material with two- and three-photon absorption, Opt. Express, 13 (2005) 9230-9234. http://dx.doi.org/10.1364/OPEX.13.009230.

[45] J. He, Y. Qu, H. Li, J. Mi, W. Ji, Three-photon absorption in ZnO and ZnS crystals, Opt. Express, 13 (2005) 9235-9247. https://doi.org/10.1364/OPEX.13.009235.

[46] B. Gu, X.Q. Huang, S.Q. Tan, M. Wang, W. Ji, Z-scan analytical theories for characterizing multiphoton absorbers, Appl. Phys. B, 95 (2009) 375-381. https://doi.org/10.1007/s00340-009-3426-y.

[47] G. Tsigaridas, M. Fakis, I. Polyzos, P. Persephonis, V. Giannetas, Z-scan analysis for high order nonlinearities through Gaussian decomposition, Opt. Commun., 225 (2003) 253-268. https://doi.org/10.1016/j.optcom.2003.08.025.

[48] G. Tsigaridas, M. Fakis, I. Polyzos, M. Tsibouri, P. Persephonis, V. Giannetas, Z-scan analysis for near-Gaussian beams through Hermite–Gaussian decomposition, J. Opt. Soc. Am. B, 20 (2003) 670-676. https://doi.org/10.1364/JOSAB.20.000670.

[49] X.-Q. Yan, Z.-B. Liu, X.-L. Zhang, W.-Y. Zhou, J.-G. Tian, Polarization dependence of Z-scan measurement: theory and experiment, Opt. Express, 17 (2009) 6397-6406. https://doi.org/10.1364/OE.17.006397.

[50] M. Samoc, A. Samoc, G.T. Dalton, M.P. Cifuentes, M.G. Humphrey, P.A. Fleitz, Multiphoton Processes in Organic Materials and Their Application, Editions des Archives Contemporaines, 2012, pp. 341-355.

[51] P. Hanczyc, M. Samoc, B. Norden, Multiphoton absorption in amyloid protein fibres, Nature Photon., 7 (2013) 969-972. https://doi.org/10.1038/nphoton.2013.282.

[52] T. Wang, N. Venkatram, J. Gosciniak, Y. Cui, G. Qian, W. Ji, D.T. Tan, Multi-photon absorption and third-order nonlinearity in silicon at mid-infrared wavelengths, Opt. Express, 21 (2013) 32192-32198. https://doi.org/10.1364/OE.21.032192.

[53] F. Kessi, H. Naima, Open Z-scan analytical model for multiphoton absorption, J. Opt., 49 (2020) 305-310. https://doi.org/10.1007/s12596-020-00615-5.

[54] P.B. Chapple, J. Staromlynska, R.G. McDuff, Z-scan studies in the thin- and the thick-sample limits, J. Opt. Soc. Am. B, 11 (1994) 975-982. https://doi.org/10.1364/JOSAB.11.000975.

[55] K.S. Bindra, S.M. Oak, K.C. Rustagi, Intensity dependence of Z-scan in semiconductor-doped glasses for separation of third and fifth order contributions in the below band gap region, Opt. Commun., 168 (1999) 219-225. https://doi.org/10.1016/S0030-4018(99)00326-0.

[56] S.R. Marder, J.E. Sohn, G.D. Stucky (Eds), Materials for Nonlinear Optics: Chemical Perspectives, American Chemical Society Washington DC, 1991.

[57] B.I. Lembrikov, Introductory Chapter: Nonlinear Optical Phenomena, in: Nonlinear Optics - Novel Results in Theory and Applications, IntechOpen, 2019.

[58] W. Kaiser, C.G.B. Garrett, Two-Photon Excitation in CaF2:Eu2+, Phys. Rev. Lett., 7 (1961) 229-231. https://doi.org/10.1103/PhysRevLett.7.229.

[59] D.A. Kleinman, Laser and Two-Photon Processes, Phys. Rev., 125 (1962) 87-88. https://doi.org/10.1103/PhysRev.125.87.

[60] M. Samoc, in: Two-Photon Absorption Measurements - establishing reference standards, Australian National University, 2007.

[61] Y.-C. Lin, P.-T. Chou, I.O. Koshevoy, T.A. Pakkanen, Studies of Two-Photon Property of Intensely Luminescent Alkynyl−Phosphine Gold(I)−Copper(I) Complexes, J. Phys. Chem. A, 113 (2009) 9270-9276. https://doi.org/10.1021/jp9040452.

[62] C.-H. Tao, H. Yang, N. Zhu, V.W.-W. Yam, S.-J. Xu, Branched Luminescent Multinuclear Platinum(II) Alkynyl Complexes: Candidates for Efficient Two-Photon Induced Luminescence, Organometallics, 27 (2008) 5453-5458. https://doi.org/10.1021/om800338x.

[63] J.E. Rogers, J.E. Slagle, D.M. Krein, A.R. Burke, B.C. Hall, A. Fratini, D.G. McLean, P.A. Fleitz, T.M. Cooper, M. Drobizhev, N.S. Makarov, A. Rebane, K.-Y. Kim, R. Farley, K.S. Schanze, Platinum Acetylide Two-Photon Chromophores, Inorg. Chem., 46 (2007) 6483-6494. https://doi.org/10.1021/ic700549n.

[64] E. W. Van Stryland, M. Sheik-Bahae, Z-scan Measurements of Optical Nonlinearities, in: M.G. Kuzyk, C.V. Dirk (Eds.) Characterization Techniques and Tabulations for Organic Nonlinear Optical Materials, CRC Press, New York, 1998, pp. 655-692.

[65] V. Singh, P. Aghamkar, Z-scan: A simple technique for determination of third-order optical nonlinearity, AIP Conf. Proc., 1675 (2015) 030095. https://doi.org/10.1063/1.4929311.

[66] M. Sheik-Bahae, M.P. Hasselbeck, Third Order Optical Nonlinearities, in: OSA Handbook of Optics, 2000.

[67] M. Sheik-Bahae, A.A. Said, T. Wei, D.J. Hagan, E.W.V. Stryland, Sensitive measurement of optical nonlinearities using a single beam, IEEE J. Quantum Electron., 26 (1990) 760-769. https://doi.org/10.1109/3.53394.

[68] W. Kaiser, C.G.B. Garrett, Two-Photon Excitation in CaF_2: Eu^{2+}, Phys. Rev. Lett., 7 (1961) 229-231. https://doi.org/10.1103/PhysRevLett.7.229.

[69] J.A. Giordmaine, P.M. Rentzepis, S.L. Shapiro, K.W. Wecht, Two-photon excitation of fluorescence by picosecond light pulses, Appl. Phys. Lett., 11 (1967) 216-218. https://doi.org/10.1063/1.1755105.

[70] M.G. Humphrey, Ruthenium Alkynyl Complexes in Non-Linear Optics, Aust. J. Chem., 71 (2018) 731-742. https://doi.org/10.1071/CH18325.

[71] J. Staromlynska, T.J. McKay, J.A. Bolger, J.R. Davy, Evidence for broadband optical limiting in a Pt:ethynyl compound, J. Opt. Soc. Am. B, 15 (1998) 1731-1736. https://doi.org/10.1364/JOSAB.15.001731.

[72] T.J. McKay, J. Staromlynska, P. Wilson, J. Davy, Nonlinear luminescence spectroscopy in a Pt:ethynyl compound, J. Appl. Phys., 85 (1999) 1337-1341. https://doi.org/10.1063/1.369264.

[73] I.R. Whittall, M.G. Humphrey, D.C.R. Hockless, B.W. Skelton, A.H. White, Organometallic Complexes for Nonlinear Optics. 2. Syntheses, Electrochemical Studies, Structural Characterization, and Computationally-Derived Molecular Quadratic Hyperpolarizabilities of Ruthenium σ-Arylacetylides: X-ray Crystal Structures of $Ru(C{\equiv}CPh)(PMe_3)_2(\eta\text{-}C_5H_5)$ and $Ru(C{\equiv}CC_6H_4NO_2\text{-}4)(L)_2(\eta\text{-}C_5H_5)$ (L = PPh_3, PMe_3), Organometallics, 14 (1995) 3970-3979. https://doi.org/10.1021/om00008a050.

[74] A.M. McDonagh, M.P. Cifuentes, I.R. Whittall, M.G. Humphrey, M. Samoc, B. Luther-Davies, D.C.R. Hockless, Organometallic complexes for non-linear optics VII. Cubic optical non-linearities of octahedral *trans*-bis{bis(diphenylphosphino)methane}ruthenium acetylide complexes; X-ray crystal structure of trans-$[Ru(C{\equiv}CPh)(4\text{-}C{\equiv}CC_6H_4NO_2)(dppm)_2]$, J. Organomet. Chem., 526 (1996) 99-103. https://doi.org/10.1016/S0022-328X(96)06469-8.

[75] I.R. Whittall, M.G. Humphrey, M. Samoc, B. Luther-Davies, Molecular Cubic Hyperpolarizabilities of Systematically Varied (Triphenylphosphane)–gold-σ-Arylalkynyl Complexes, Angew. Chem. Int. Ed., 36 (1997) 370-371. https://doi.org/10.1002/anie.199703701.

[76] A.M. McDonagh, M.G. Humphrey, M. Samoc, B. Luther-Davies, Organometallic Complexes for Nonlinear Optics. 17. Synthesis, Third-Order Optical Nonlinearities, and Two-Photon Absorption Cross Section of an Alkynylruthenium Dendrimer, Organometallics, 18 (1999) 5195-5197. https://doi.org/10.1021/om9908130.

[77] A. Colombo, C. Dragonetti, V. Guerchais, D. Roberto, An excursion in the second-order nonlinear optical properties of platinum complexes, Coord. Chem. Rev., 446 (2021) 214113. https://doi.org/10.1016/j.ccr.2021.214113.

[78] M.G. Humphrey, T. Schwich, P.J. West, M.P. Cifuentes, M. Samoc, Nonlinear Optical Properties of Coordination and Organometallic Complexes, in: J. Reedijk, K. Poeppelmeier (Eds.) Comprehensive Inorganic Chemistry II, Elsevier, Amsterdam, 2013, vol. 8, pp. 781-835.

[79] G. Grelaud, M.P. Cifuentes, F. Paul, M.G. Humphrey, Group 8 metal alkynyl complexes for nonlinear optics, J. Organomet. Chem., 751 (2014) 181-200. https://doi.org/10.1016/j.jorganchem.2013.10.008.

[80] A. Colombo, C. Dragonetti, V. Guerchais, C. Hierlinger, E. Zysman-Colman, D. Roberto, A trip in the nonlinear optical properties of iridium complexes, Coord. Chem. Rev., 414 (2020) 213293. https://doi.org/10.1016/j.ccr.2020.213293.

[81] B. Babgi, L. Rigamonti, M.P. Cifuentes, T.C. Corkery, M.D. Randles, T. Schwich, S. Petrie, R. Stranger, A. Teshome, I. Asselberghs, K. Clays, M. Samoc, M.G. Humphrey, Length-dependent convergence and saturation behavior of electrochemical, linear optical, quadratic nonlinear optical, and cubic nonlinear optical properties of dipolar alkynylruthenium complexes with oligo(phenyleneethynylene) bridges, J. Am. Chem. Soc., 131 (2009) 10293-10307. https://doi.org/10.1021/ja902793z.

[82] M. Morshedi, M.S. Kodikara, T.C. Corkery, S.K. Hurst, S.S. Chavan, E. Kulasekera, R. Stranger, M. Samoc, S. Van Cleuvenbergen, I. Asselberghs, K. Clays, M.P. Cifuentes, M.G. Humphrey, Quadratic and Cubic Optical Nonlinearities of Y-Shaped and Distorted-H-Shaped Arylalkynylruthenium Complexes, Chem. Eur. J., 24 (2018) 16332-16341. https://doi.org/10.1002/chem.201803696.

[83] A.M. McDonagh, M.G. Humphrey, M. Samoc, B. Luther-Davies, S. Houbrechts, T. Wada, H. Sasabe, A. Persoons, Organometallic Complexes for Nonlinear Optics. 16. Second and Third Order Optical Nonlinearities of Octopolar Alkynylruthenium Complexes, J. Am. Chem. Soc., 121 (1999) 1405-1406. http://dx.doi.org/10.1021/ja982965c.

[84] S.K. Hurst, M.P. Cifuentes, J.P.L. Morrall, N.T. Lucas, I.R. Whittall, M.G. Humphrey, I. Asselberghs, A. Persoons, M. Samoc, B. Luther-Davies, A.C. Willis, Organometallic Complexes for Nonlinear Optics. 22. Quadratic and Cubic Hyperpolarizabilities of *trans*-Bis(bidentate phosphine)ruthenium σ-Arylvinylidene and σ-Arylalkynyl Complexes, Organometallics, 20 (2001) 4664-4675. https://doi.org/10.1021/om0101700.

[85] L. Rigamonti, B. Babgi, M.P. Cifuentes, R.L. Roberts, S. Petrie, R. Stranger, S. Righetto, A. Teshome, I. Asselberghs, K. Clays, M.G. Humphrey, Organometallic complexes for nonlinear optics. 43. Quadratic optical nonlinearities of dipolar alkynylruthenium complexes with phenyleneethynylene/phenylenevinylene bridges, Inorg. Chem., 48 (2009) 3562-3572. https://doi.org/10.1021/ic801953z.

[86] S.K. Hurst, M.P. Cifuentes, M.G. Humphrey, A rapid convergent approach to organometallic dendrimers: Sterically controlled dendron synthesis, Organometallics, 21 (2002) 2353-2255. https://doi.org/10.1021/om0202120

[87] K.A. Green, P.V. Simpson, T.C. Corkery, M.P. Cifuentes, M. Samoc, M.G. Humphrey, Divergent Synthesis of Ruthenium Alkynyl Dendrimers and a Two-Photon Absorption Cross-Section Dendritic Effect, Macromol. Rapid Commun., 33 (2012) 573-578. https://doi.org/10.1002/marc.201100770.

[88] P.V. Simpson, L.A. Watson, A. Barlow, G. Wang, M.P. Cifuentes, M.G. Humphrey, Record Multiphoton Absorption Cross-Sections by Dendrimer Organometalation, Angew. Chem. Int. Ed., 55 (2016) 2387-2391. https://doi.org/10.1002/anie.201509223.

[89] K. Mitra, C.E. Lyons, M. C.T. Hartman, A Platinum(II) Complex of Heptamethine Cyanine for Photoenhanced Cytotoxicity and Cellular Imaging in Near-IR Light, Angew. Chem. Int. Ed., 57 (2018) 10263-10267. https://doi.org/10.1002/anie.201806911.

[90] R.E. Doherty, I.V. Sazanovich, L.K. McKenzie, A.S. Stasheuski, R. Coyle, E. Baggaley, S. Bottomley, J.A. Weinstein, H.E. Bryant, Photodynamic killing of cancer cells by a Platinum(II) complex with cyclometallating ligand, Sci. Rep. 6 (2016) 22668. DOI: 10.1038/srep22668.

[91] T.P. Seifert, V.R. Naina, T.J. Feuerstein, N.D. Knöfel, P.W. Roesky, Molecular gold strings: aurophilicity, luminescence and structure–property correlations, Nanoscale, 12 (2020) 20065-20088. DOI: 10.1039/D0NR04748A.

[92] J.H. Kim, E. Reeder, S. Parkin, S.G. Awuah, Gold(I/III)-Phosphine Complexes as Potent Antiproliferative Agents, Sci. Rep. 9 (2019) 12335. https://doi.org/10.1038/s41598-019-48584-5.

[93] B.Đ. Glišić, M.I. Djuran, Gold complexes as antimicrobial agents: an overview of different biological activities in relation to the oxidation state of the gold ion and the ligand structure, Dalton Trans., 43 (2014) 5950-5969. https://doi.org/10.1039/C4DT00022F.

[94] J. Du, M.S. Kodikara, G.J. Moxey, M. Morshedi, A. Barlow, C. Quintana, G. Wang, R. Stranger, C. Zhang, M.P. Cifuentes, M.G. Humphrey, Quadratic and cubic hyperpolarizabilities of nitro-phenyl/-naphthalenyl/-anthracenyl alkynyl complexes, Dalton Trans, 47 (2018) 4560-4571. https://doi.org/10.1039/C8DT00155C.

[95] A.A. Melekhova, D.V. Krupenya, V.V. Gurzhiy, A.S. Melnikov, P.Y. Serdobintsev, S.I. Selivanov, S.P. Tunik, Synthesis, characterization, luminescence and non-linear optical properties of diimine platinum(II) complexes with arylacetylene ligands, J. Organomet. Chem., 763-764 (2014) 1-5. https://doi.org/10.1016/j.jorganchem.2014.04.002.

[96] Y. Fan, D. Zhao, Triangular Platinum(II) Metallacycles: Syntheses, Photophysics, and Nonlinear Optics, ACS Appl. Mater. Interfaces, 7 (2015) 6162-6171. https://doi.org/10.1021/am509074m.

[97] Y. Wang, X. Shi, H. Fang, Z. Han, H. Yuan, Z. Zhu, L. Dong, Z. Guo, X. Wang, Platinum-Based Two-Photon Photosensitizer Responsive to NIR Light in Tumor Hypoxia Microenvironment, J. Med. Chem., 65 (2022), 11, 7786-7798. https://doi.org/10.1021/acs.jmedchem.2c00141.

[98] S.K. Hurst, M.P. Cifuentes, A.M. McDonagh, M.G. Humphrey, M. Samoc, B. Luther-Davies, I. Asselberghs, A. Persoons, Organometallic complexes for nonlinear optics, J. Organomet. Chem., 642 (2002) 259-267. https://doi.org/10.1016/S0022-328X(01)01281-5.

[99] T.R. Ensley, R.M. O'Donnell, J.J. Mihaly, J.E. Haley, T.A. Grusenmeyer, T.G. Gray, Two-photon absorption characterization and comparison of Au(I) fluorenyl benzothiazole complexes in the visible wavelength regime, Appl. Opt., 60 (2021) G199-G206. https://doi.org/10.1364/AO.427968.

[100] B. Gao, L.M. Mazur, M. Morshedi, A. Barlow, H. Wang, C. Quintana, C. Zhang, M. Samoc, M.P. Cifuentes, M.G. Humphrey, Exceptionally large two- and three-photon absorption cross-sections by OPV organometalation, Chem. Commun., 52 (2016) 8301-8304. https://doi.org/10.1039/C6CC02560A.

[101] M. Morshedi, M.S. Kodikara, T.C. Corkery, S.K. Hurst, S.S. Chavan, E. Kulasekera, R. Stranger, M. Samoc, S. Van Cleuvenbergen, I. Asselberghs, K. Clays, M.P. Cifuentes, M.G. Humphrey, Quadratic and Cubic Optical Nonlinearities of Y-Shaped and Distorted-H-Shaped Arylalkynylruthenium Complexes, Chem. Eur. J., 24 (2018) 16332-16341.

https://doi.org/10.1002/chem.201803696.

[102] Z. Chen, C.J. Jeffery, M. Morshedi, G.J. Moxey, A. Barlow, X. Yang, B.A. Babgi, G.T. Dalton, M.D. Randles, M.K. Smith, C. Zhang, M. Samoc, M.P. Cifuentes, M.G. Humphrey, Syntheses, Electrochemical, Linear Optical, and Cubic Nonlinear Optical Properties of Ruthenium-Alkynyl-Functionalized Oligo(phenylenevinylene) Stars, ChemPlusChem, 80 (2015) 1329-1340. https://doi.org/10.1002/cplu.201500220.

[103] S. Drouet, A. Merhi, D. Yao, M.P. Cifuentes, M.G. Humphrey, M. Wielgus, J. Olesiak-Banska, K. Matczyszyn, M. Samoc, F. Paul, C.O. Paul-Roth, Cubic nonlinear optical properties of new zinc tetraphenyl porphyrins peripherally functionalized with electron-rich Ru(II) alkynyl substituents, Tetrahedron, 68 (2012) 10351-10359. https://doi.org/10.1016/j.tet.2012.09.108.

[104] T.M. Cooper, J.E. Haley, D.M. Krein, A.R. Burke, J.E. Slagle, A. Mikhailov, A. Rebane, Two-Photon Spectroscopy of a Series of Platinum Acetylides: Conformation-Induced Ground-State Symmetry Breaking, J. Phys. Chem. A, 121 (2017) 5442-5449. https://doi.org/10.1021/acs.jpca.7b04784.

[105] A. Rebane, M. Drobizhev, N.S. Makarov, G. Wicks, P. Wnuk, Y. Stepanenko, J.E. Haley, D.M. Krein, J.L. Fore, A.R. Burke, J.E. Slagle, D.G. McLean, T.M. Cooper, Symmetry Breaking in Platinum Acetylide Chromophores Studied by Femtosecond Two-Photon Absorption Spectroscopy, J. Phys. Chem. A, 118 (2014) 3749-3759. https://doi.org/10.1021/jp5009658.

[106] M.G. Vivas, L. De Boni, T.M. Cooper, C.R. Mendonca, Understanding the Two-Photon Absorption Spectrum of PE2 Platinum Acetylide Complex, J. Phys. Chem. A, 118 (2014) 5608-5613. https://doi.org/10.1021/jp503318u.

[107] M.G. Vivas, L. De Boni, T.M. Cooper, C.R. Mendonca, Interpreting Strong Two-Photon Absorption of PE3 Platinum Acetylide Complex: Double Resonance and Excited State Absorption, ACS Photonics, 1 (2014) 106-113. https://doi.org/10.1021/ph4000357.

[108] F. Wei, X. Huang, Z. Lian, Y. Zhu, F. Guo, Computational and experimental assessment on the nonlinear optical properties of platinum(II) arylacetylides with donor-acceptor structures, J. Organomet. Chem., 904 (2019) 121003. https://doi.org/10.1016/j.jorganchem.2019.121003.

[109] A.H. Shelton, S.R. Valandro, R.S. Price, G.G. Dubinina, K.A. Abboud, G. Wicks, A. Rebane, M. Younus, K.S. Schanze, Stereochemical Effects on Platinum Acetylide Two-Photon Chromophores, J. Phys. Chem. A, 123 (2019) 9382-9393. https://doi.org/10.1021/acs.jpca.9b07823.

[110] M. Pawlicki, H.A. Collins, R.G. Denning, H.L. Anderson, Two-Photon Absorption and the Design of Two-Photon Dyes, Angew. Chem. Int. Ed., 48 (2009) 3244-3266. https://doi.org/10.1002/anie.200805257.

[111] G.G. Dubinina, R.S. Price, K.A. Abboud, G. Wicks, P. Wnuk, Y. Stepanenko, M. Drobizhev, A. Rebane, K.S. Schanze, Phenylene Vinylene Platinum(II) Acetylides with Prodigious Two-Photon Absorption, J. Am. Chem. Soc., 134 (2012) 19346-19349. https://doi.org/10.1021/ja309393c.

[112] R.W. Winkel, G.G. Dubinina, K.A. Abboud, K.S. Schanze, Photophysical properties of *trans*-platinum acetylide complexes featuring N-heterocyclic carbene ligands, Dalton Trans, 43 (2014) 17712-17720. https://doi.org/10.1039/C4DT01520G.

[113] S. Goswami, R.W. Winkel, K.S. Schanze, Photophysics and Nonlinear Absorption of Gold(I) and Platinum(II) Donor–Acceptor–Donor Chromophores, Inorg. Chem., 54 (2015) 10007-10014. https://doi.org/10.1021/acs.inorgchem.5b01767.

[114] B.A. Babgi, A. Al-Hindawi, G.J. Moxey, F.I. Abdul Razak, M.P. Cifuentes, E. Kulasekera, R. Stranger, A. Teshome, I. Asselberghs, K. Clays, M.G. Humphrey, Organometallic complexes for nonlinear optics. 52. Syntheses, structural, spectroscopic, quadratic nonlinear optical, and theoretical studies of Ru($C_2C_6H_4$R-4)(κ^2-dppf)(η^5-C_5H_5) (R = H, NO_2), J. Organomet. Chem., 730 (2013) 108-115. https://doi.org/10.1016/j.jorganchem.2012.12.039.

[115] C.-L. Ho, Z.-Q. Yu, W.-Y. Wong, Multifunctional polymetallaynes: properties, functions and applications, Chem. Soc. Rev., 45 (2016) 5264-5295. https://doi.org/10.1039/C6CS00226A.

[116] S. Goswami, G. Wicks, A. Rebane, K.S. Schanze, Photophysics and non-linear absorption of Au(I) and Pt(II) acetylide complexes of a thienyl-carbazole chromophore, Dalton Trans, 43 (2014) 17721-17728. https://doi.org/10.1039/C4DT02123A.

[117] F. Juvenal, H. Lei, P.-L. Karsenti, P.D. Harvey, Drastic effect of the substituent on the anthraquinone diimine moiety on the properties of the push-pull *trans*-bis(phosphine)bis(phenylalkynyl)platinum(II)-containing polymers, J. Organomet. Chem., 896 (2019) 24-31. https://doi.org/10.1016/j.jorganchem.2019.05.024.

[118] Y. Du, N. Dong, M. Zhang, B. Jiang, N. Sun, Y. Luo, S. Zhang, G. Wang, J. Wang, Poly(arylene ether)s based on platinum(II) acetylide complexes: synthesis and photophysical and nonlinear absorption properties, J. Mater. Chem. C, 6 (2018) 7317-7325. https://doi.org/10.1039/C8TC01303A.

[119] T. Schwich, A. Barlow, M.P. Cifuentes, J. Szeremeta, M. Samoc, M.G. Humphrey, Stellar Multi-Photon Absorption Materials: Beyond the Telecommunication Wavelength Band, Chem. Eur. J., 23 (2017) 8395-8399. https://doi.org/10.1002/chem.201702039.

[120] P. Xie, L. Wang, Z. Huang, F. Guo, Q. Jin, Nonlinear Optical Properties of Conjugated Platinum(II) Acetylides with Multibranched Donor–Acceptor Structures, Eur. J. Inorg. Chem., (2014) 2544-2551. https://doi.org/10.1002/ejic.201402043.

[121] A.M. McDonagh, C.E. Powell, J.P. Morrall, M.P. Cifuentes, M.G. Humphrey, Convergent Synthesis of Alkynylbis(bidentate phosphine)ruthenium Dendrimers, Organometallics, 22 (2003) 1402-1413. http://dx.doi.org/10.1021/om020975n.

[122] C.E. Powell, J.P. Morrall, S.A. Ward, M.P. Cifuentes, E.G.A. Notaras, M. Samoc, M.G. Humphrey, Dispersion of the Third-Order Nonlinear Optical Properties of an Organometallic Dendrimer, J. Am. Chem. Soc., 126 (2004) 12234-12235. http://dx.doi.org/10.1021/ja048608l.

[123] M.P. Cifuentes, C.E. Powell, J.P. Morrall, A.M. McDonagh, N.T. Lucas, M.G. Humphrey, M. Samoc, S. Houbrechts, I. Asselberghs, K. Clays, A. Persoons, T. Isoshima, Electrochemical, Spectroelectrochemical, and Molecular Quadratic and Cubic Nonlinear Optical Properties of Alkynylruthenium Dendrimers1, J. Am. Chem. Soc., 128 (2006) 10819-10832. http://dx.doi.org/10.1021/ja062246v

[124] L. Zhang, M. Morshedi, M.G. Humphrey, Outstanding Multi-Photon Absorption at π-Delocalizable Metallodendrimers, Angew. Chem. Int. Ed., 61 (2022) e202116181. https://doi.org/10.1002/anie.202116181

[125] M.G. Kuzyk, J. Chem. Phys., 119 (2003) 8327-8334. https://doi.org/10.1063/1.1611474

[126] T. Schwich, M.P. Cifuentes, P.A. Gugger, M. Samoc, M.G. Humphrey, Adv. Mater., 23 (2011) 1433-1455. https://doi.org/10.1002/adma.200803669

[127] F. Zhou, X. Ran, D. Fan, S. Lu, W. Ji, Perovskites: Multiphoton Absorption and Applications, Adv. Opt. Mater., 9 (2021) 2100292. https://doi.org/10.1002/adom.202100292.

[128] M. Samoc, J.P. Morrall, G.T. Dalton, M.P. Cifuentes, M.G. Humphrey, Two-Photon and Three-Photon Absorption in an Organometallic Dendrimer, Angew. Chem. Int. Ed., 46 (2007) 731-733. https://doi.org/10.1002/anie.200602341.

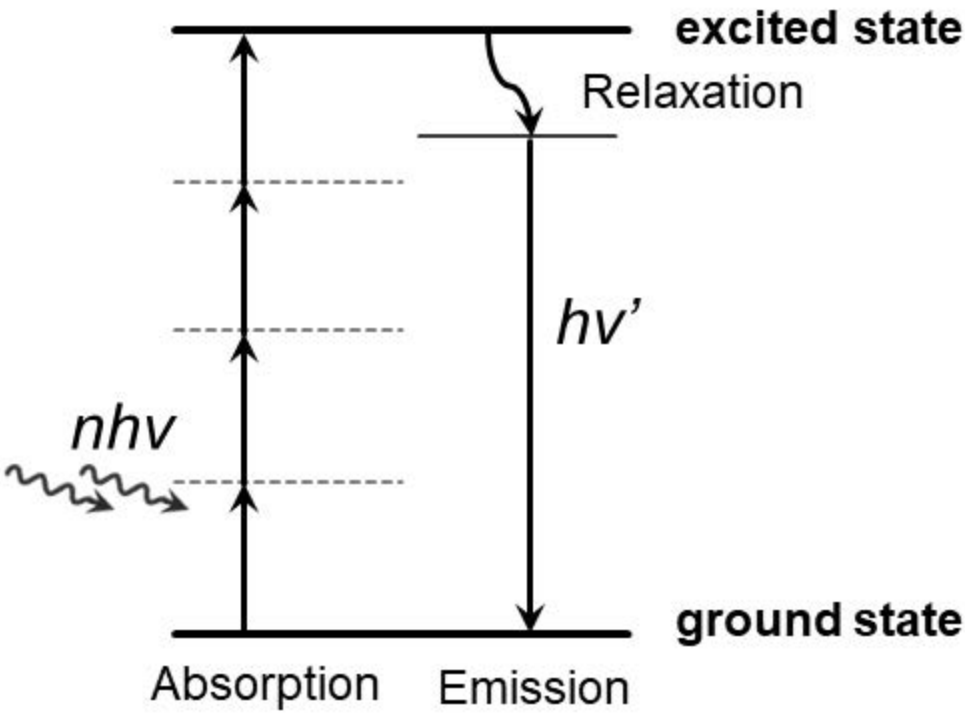
excited state
Relaxation
hv'
nhv
ground state
Absorption
Emission

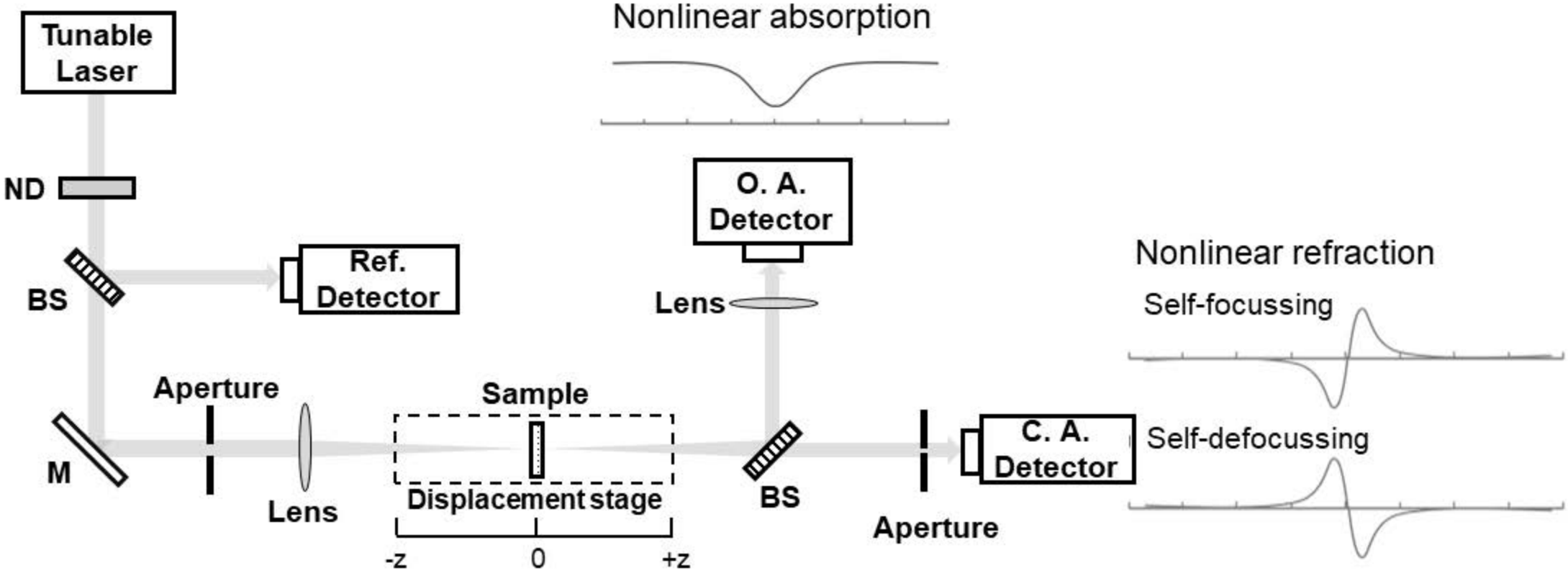
Tunable Laser
ND
BS
Ref. Detector
M
Aperture
Lens
Sample
Displacement stage
-z
0
+z
BS
Lens
O. A. Detector
Nonlinear absorption
Aperture
C. A. Detector
Nonlinear refraction
Self-focussing
Self-defocussing

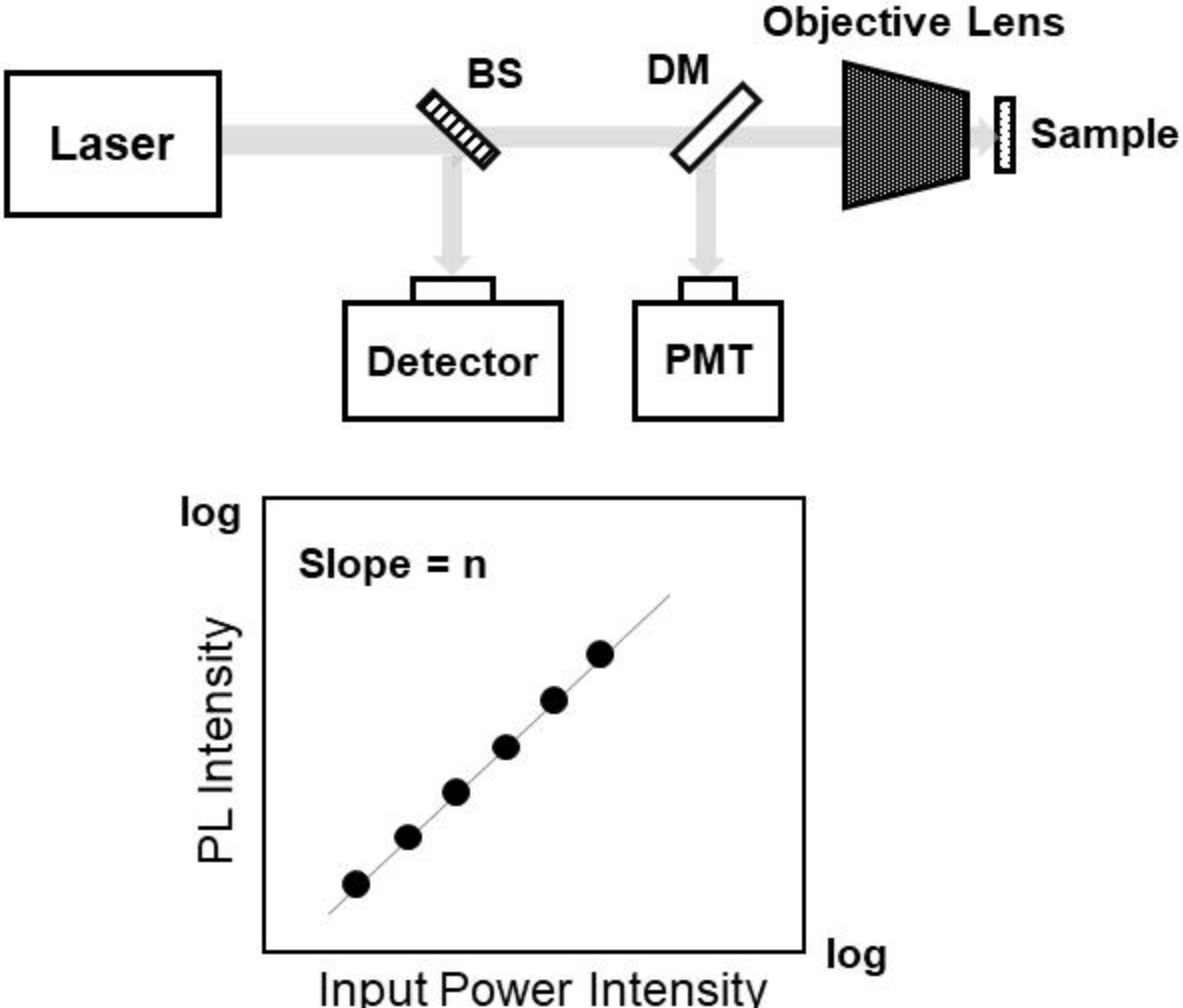
Objective Lens
BS
DM
Laser
Sample
Detector
PMT
log
Slope = n
PL Intensity
log
Input Power Intensity

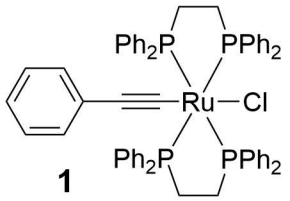

1

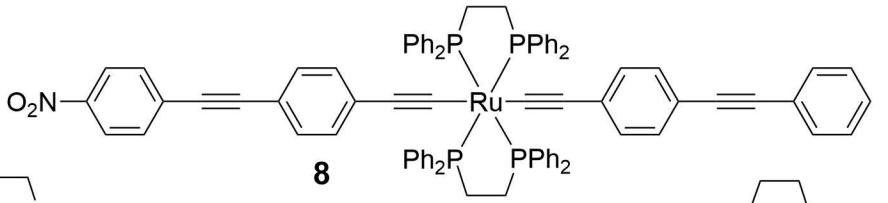

8

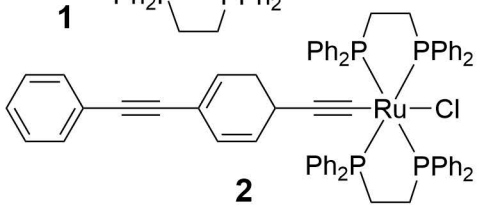

2

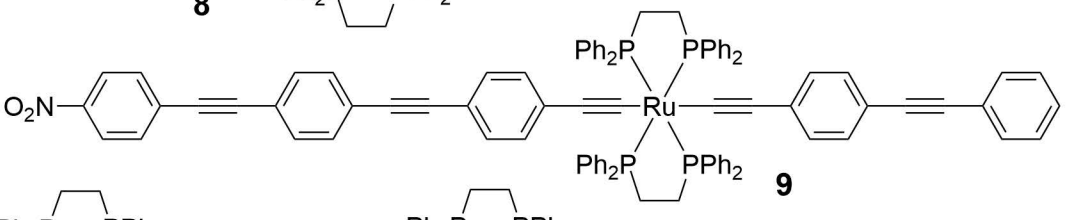

9

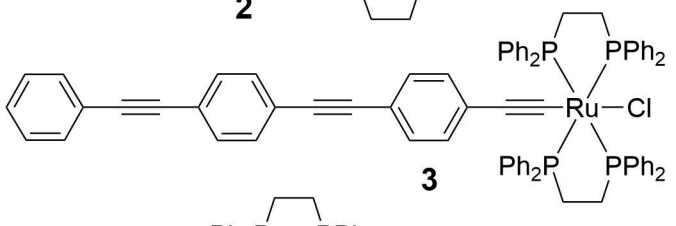

3

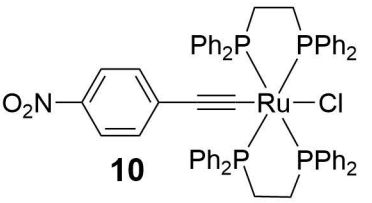

10

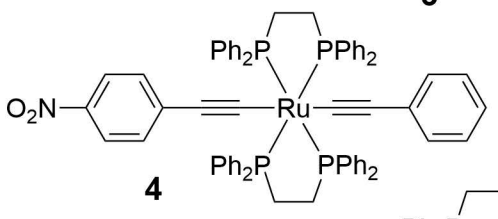

4

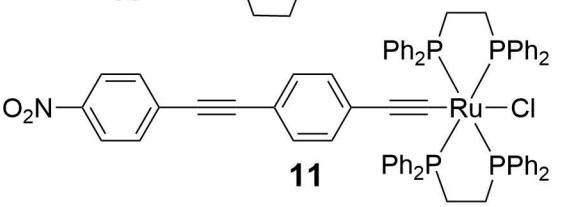

11

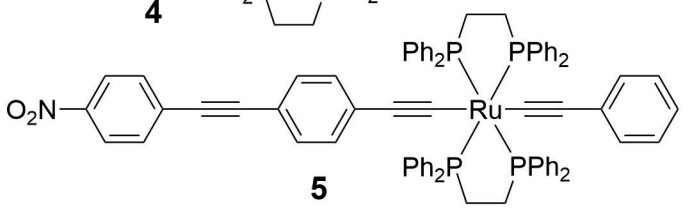

5

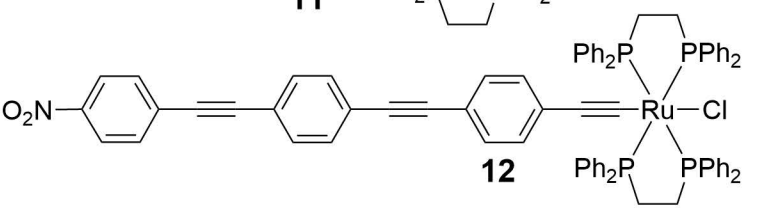

12

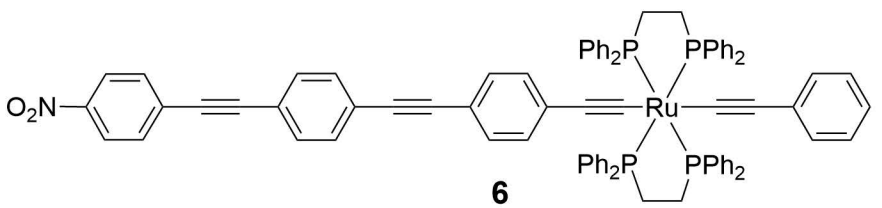

6

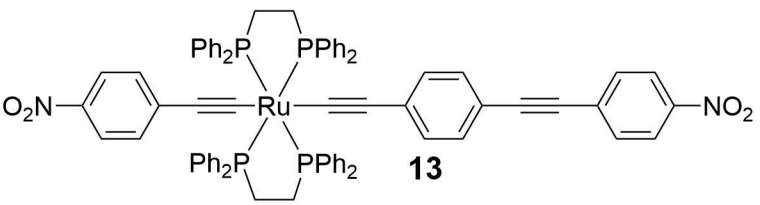

13

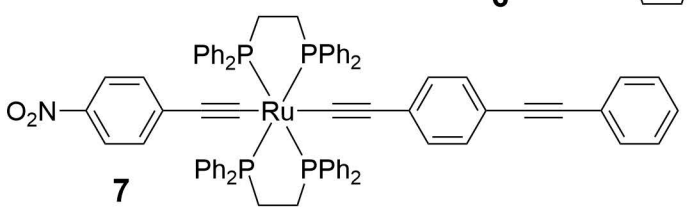

7

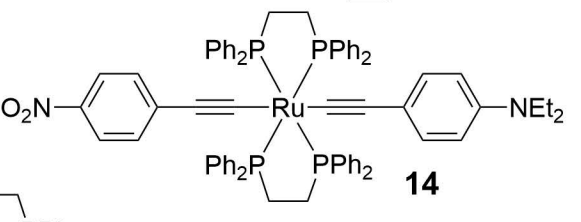

14

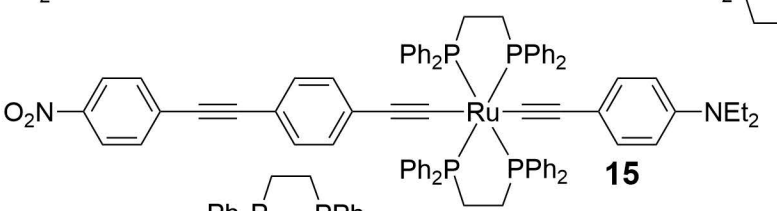

15

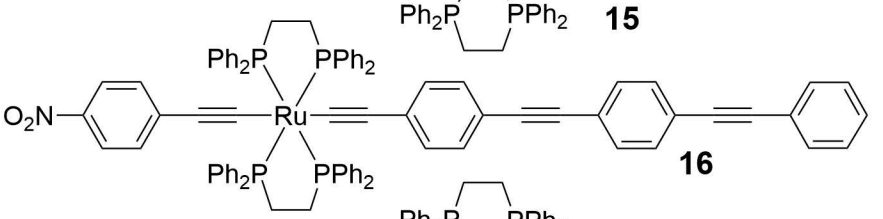

16

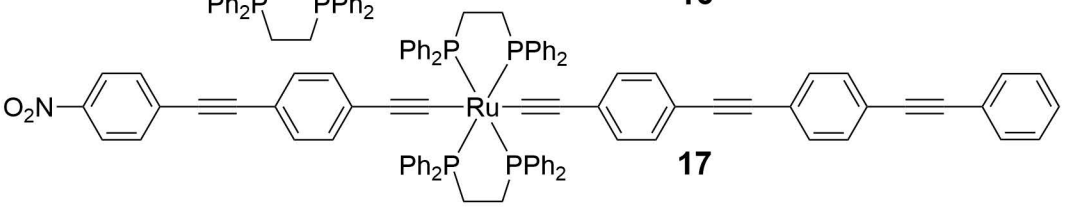

17

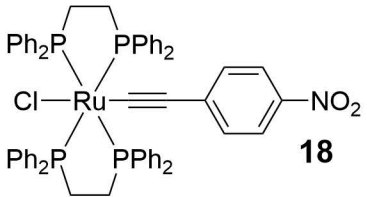

18

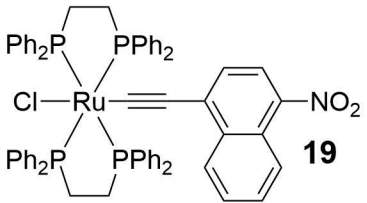

19

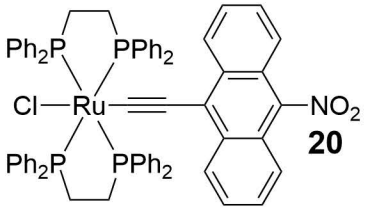

20

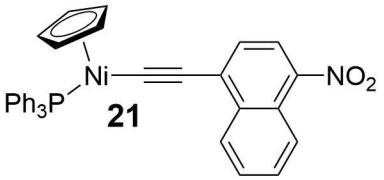

21

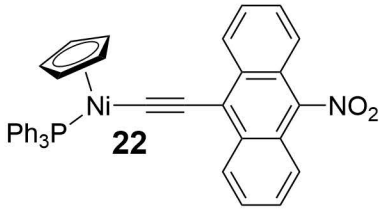

22

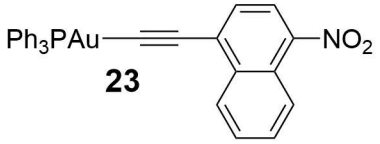

23

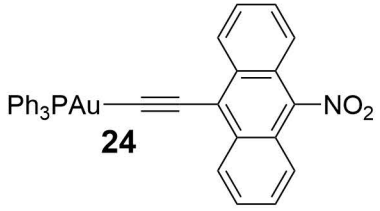

24

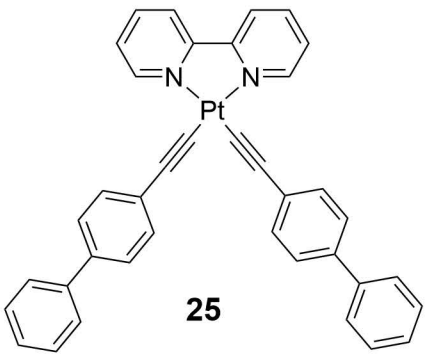

25

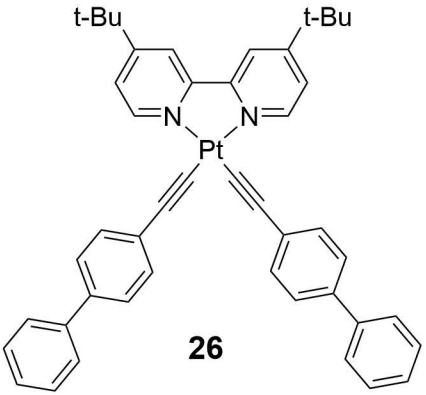

26

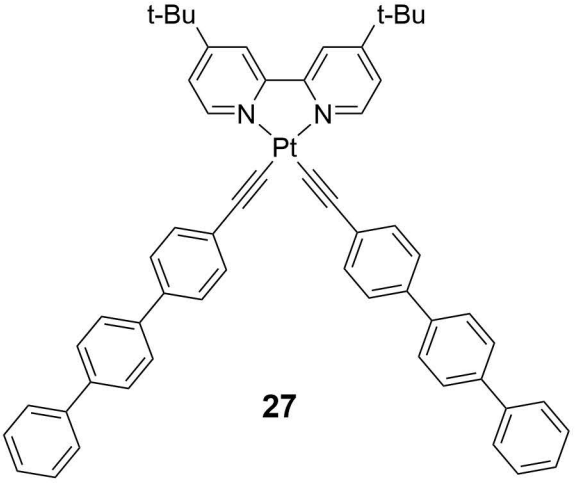

27

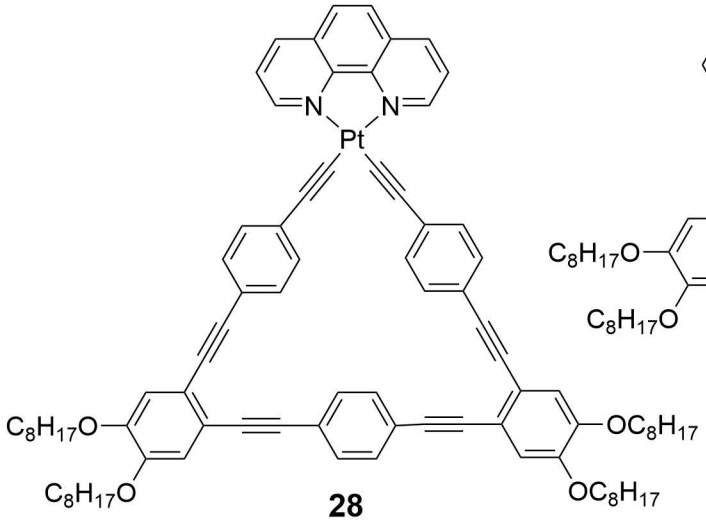

28

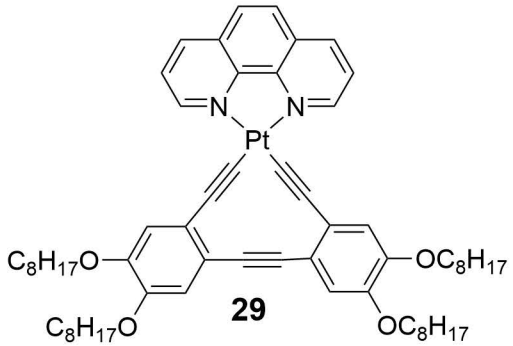

29

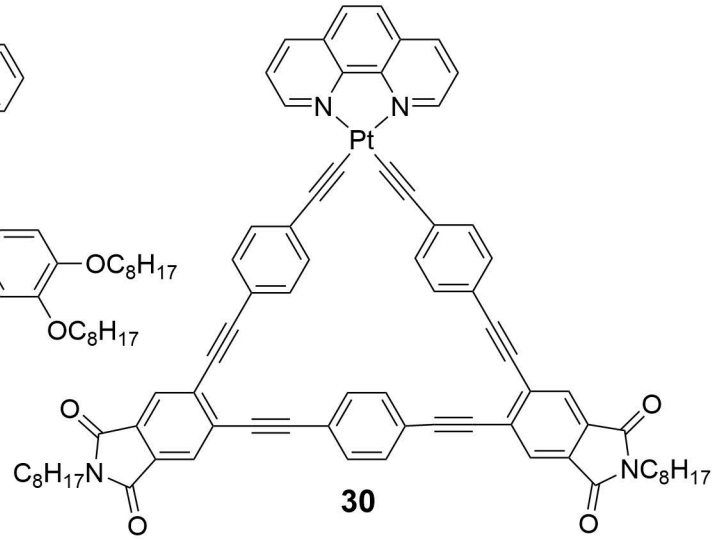

30

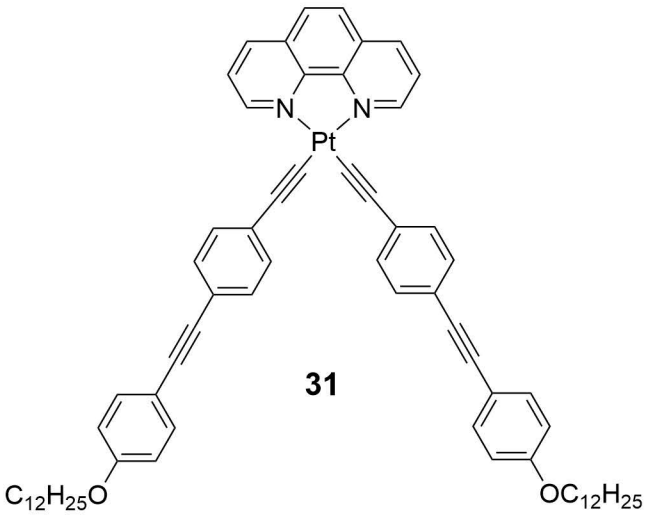

31

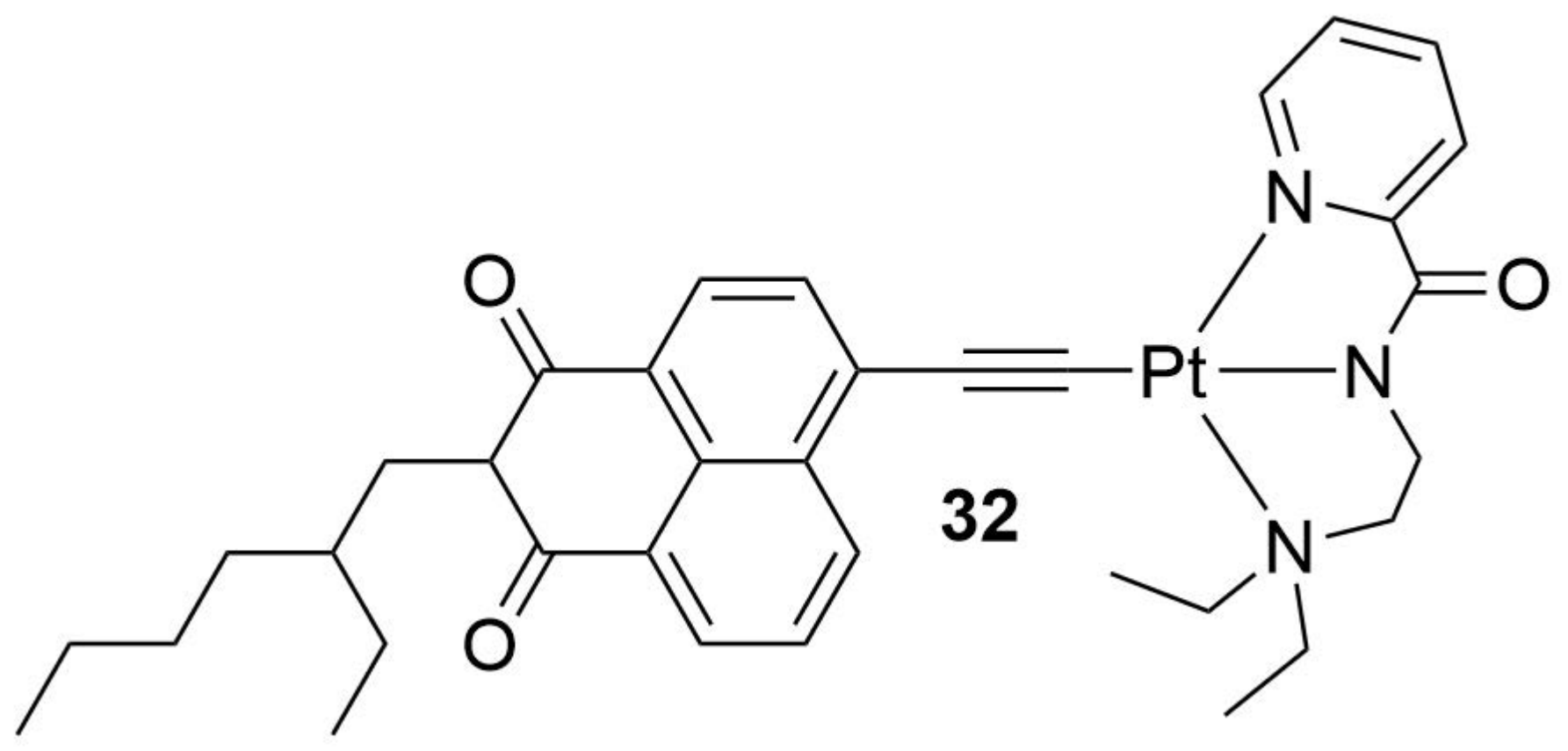

32

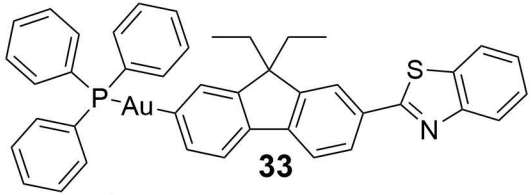

33

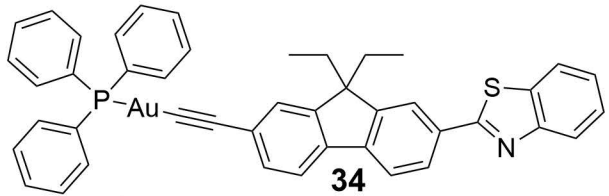

34

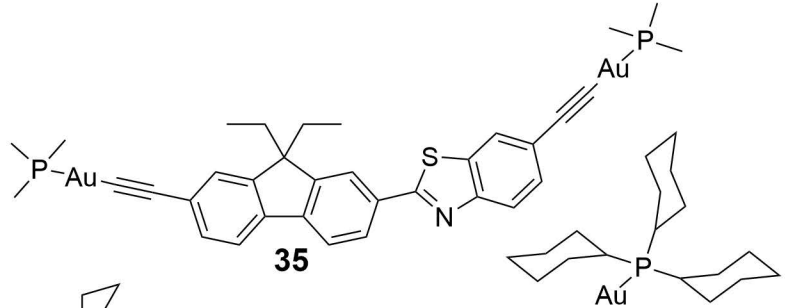

35

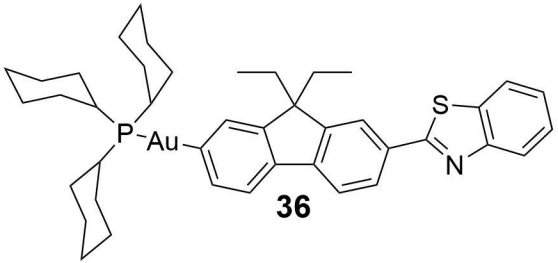

36

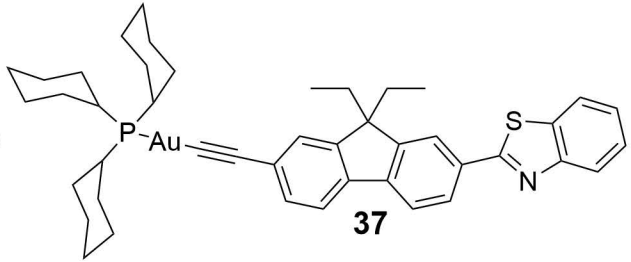

37

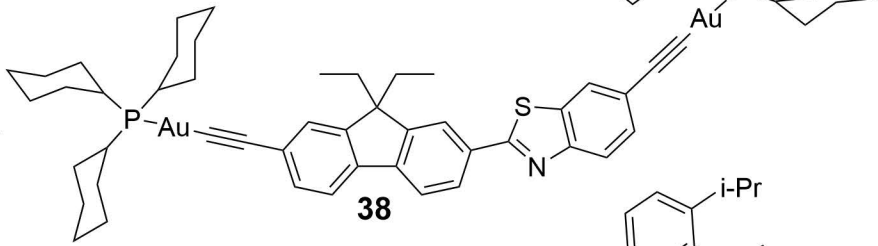

38

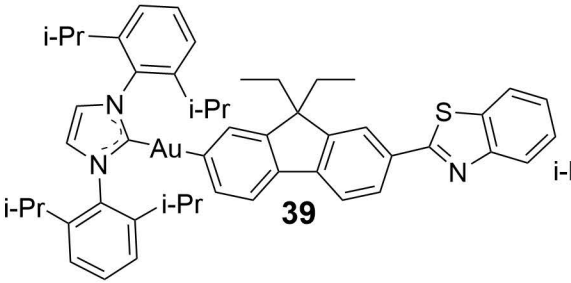

39

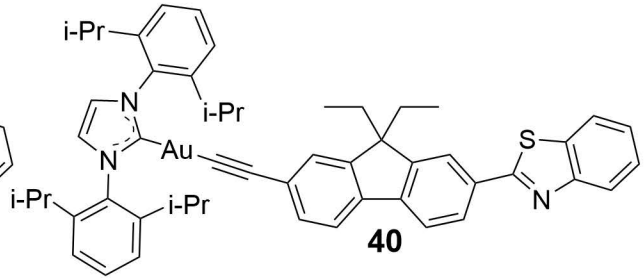

40

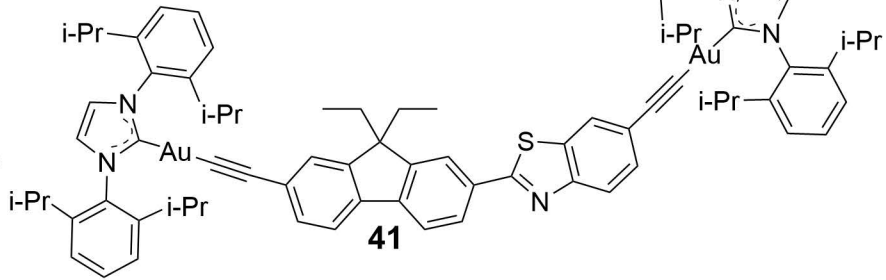

41

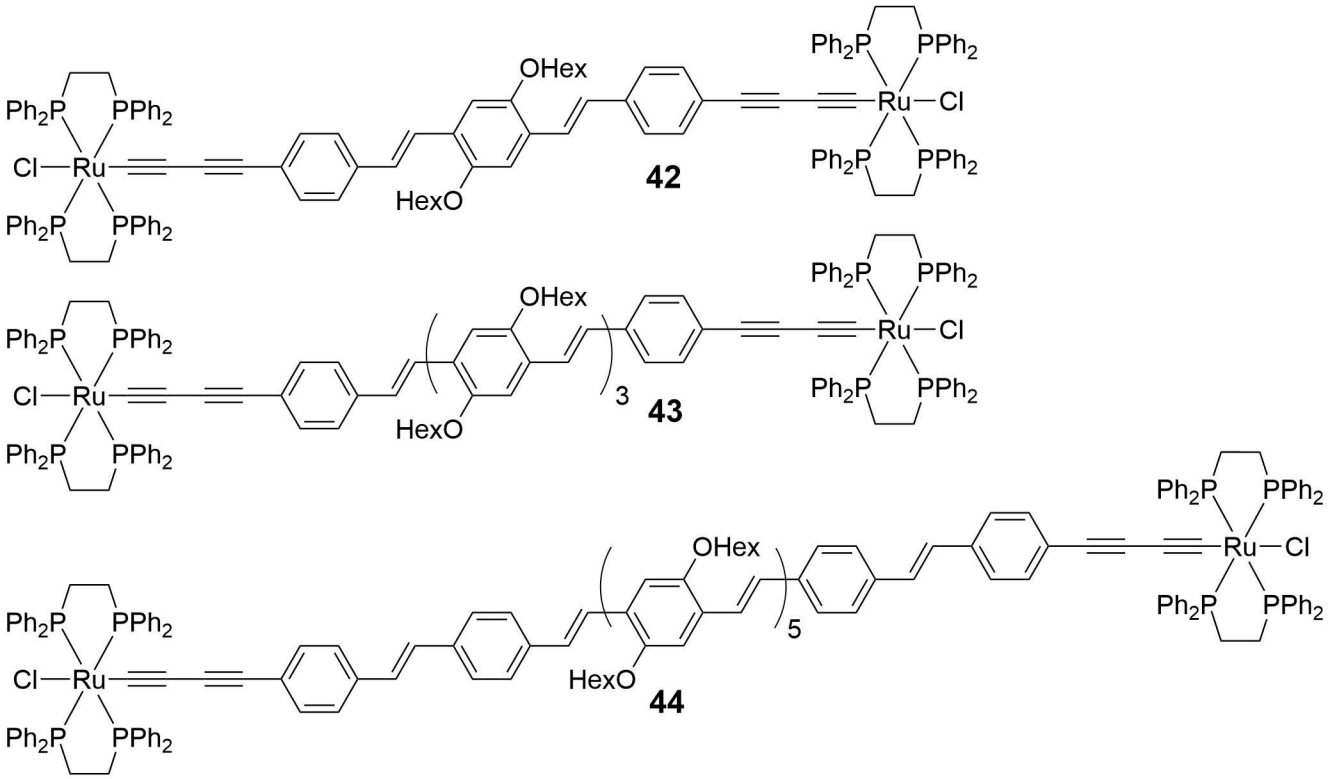
Ph2P
PPh2
Cl
Ru
OHex
HexO
42
43
3
44
5

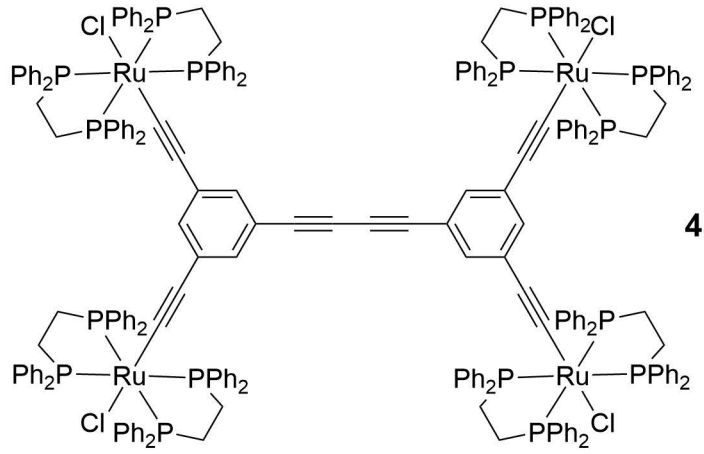

45

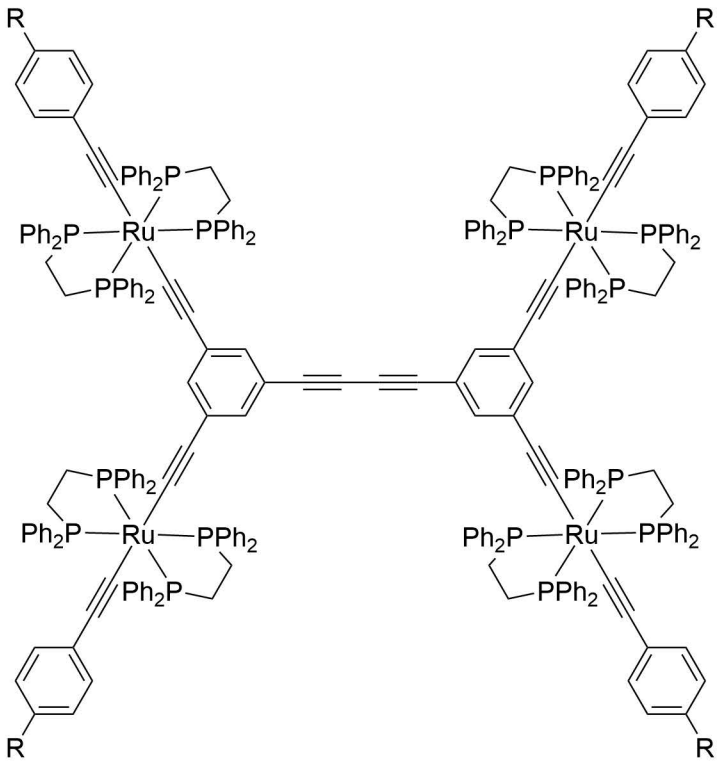

46 R = H
47 R = NO_2
48 R = NEt_2

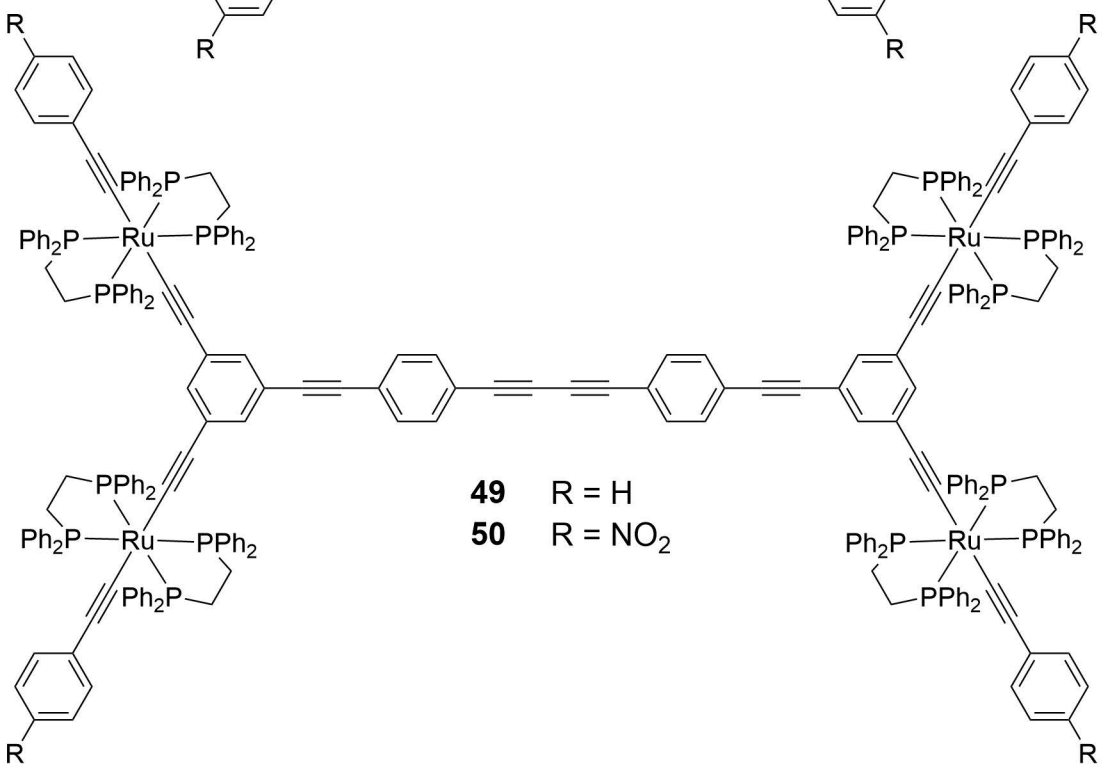

49 R = H
50 R = NO_2

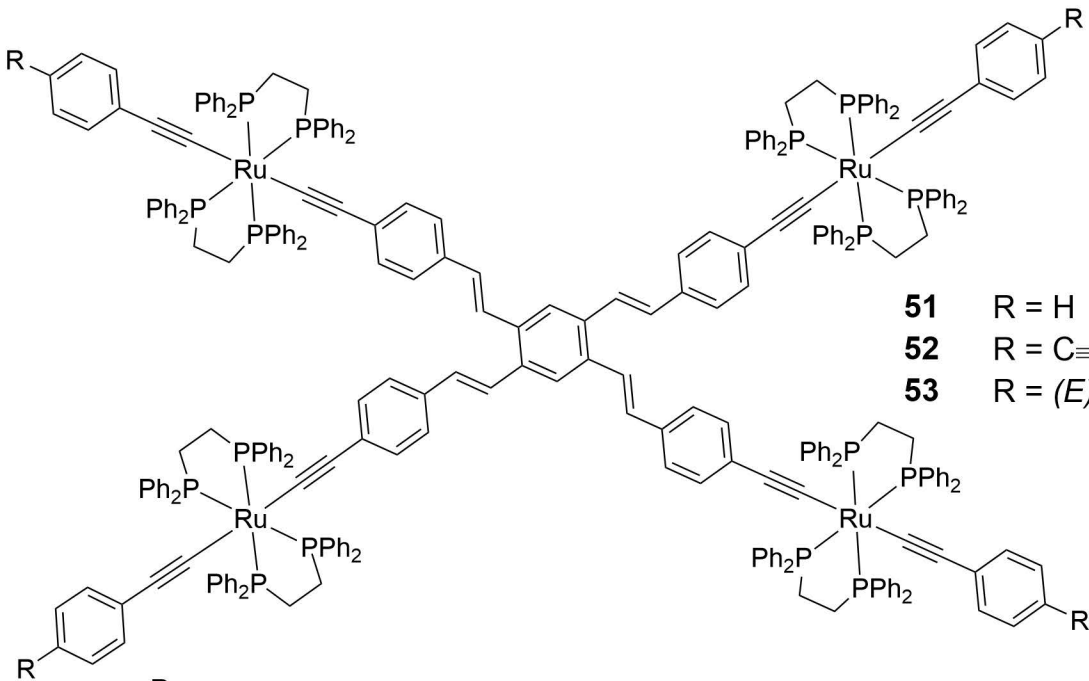

51 R = H
52 R = C≡CC$_6$H$_3$Et$_2$-3,5
53 R = *(E)*-C=CHC$_6$H$_4$*t*Bu-4

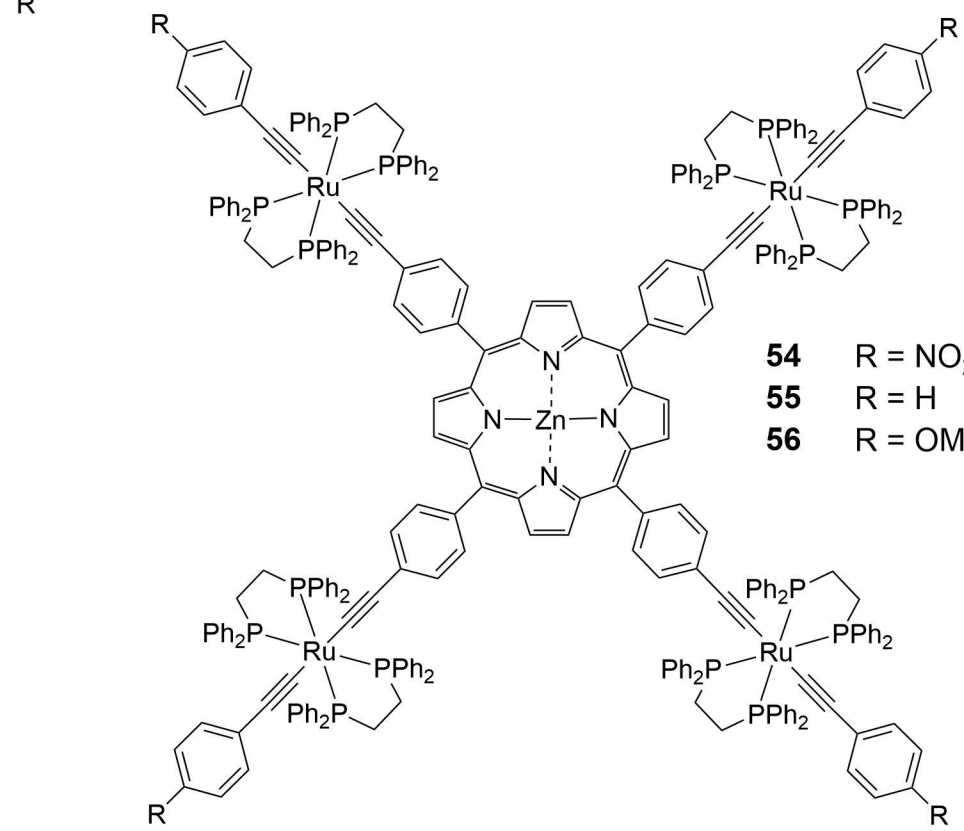

54 R = NO_2
55 R = H
56 R = OMe

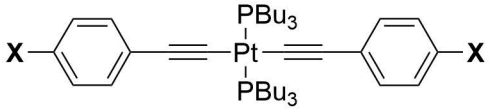

a

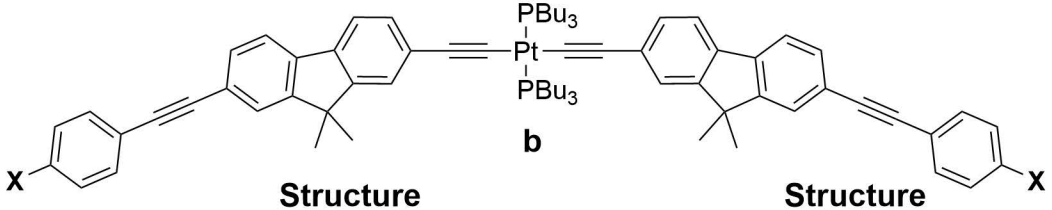

b

Structure			Structure		
X = NH_2	**a**	**57**	**X** = F	**a**	**69**
	b	**58**		**b**	**70**
X = OCH_3	**a**	**59**	**X** = benzothiazole	**a**	**71**
	b	**60**		**b**	**72**
X = NPh_2	**a**	**61**	**X** = CF_3	**a**	**73**
	b	**62**		**b**	**74**
X = t-Bu	**a**	**63**	**X** = CN	**a**	**75**
	b	**64**		**b**	**76**
X = CH_3	**a**	**65**	**X** = NO_2	**a**	**77**
	b	**66**		**b**	**78**
X = H	**a**	**67**			
	b	**68**			

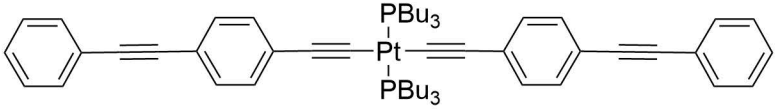

79

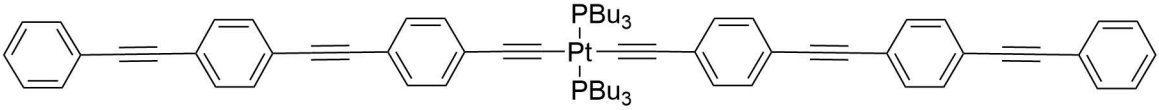

80

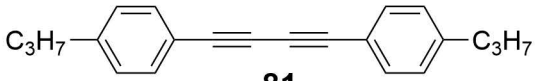

81

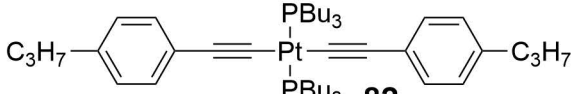

82

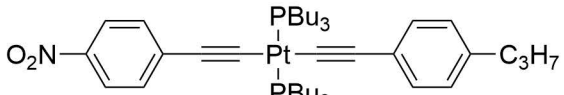

83

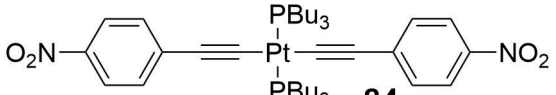

84

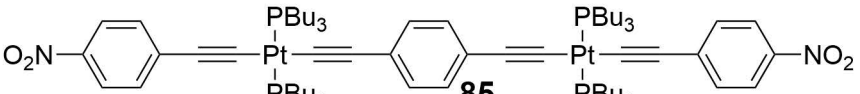

85

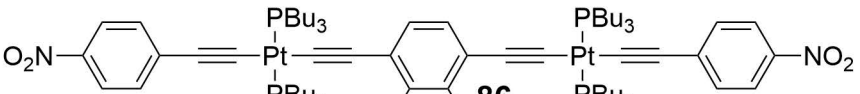

86

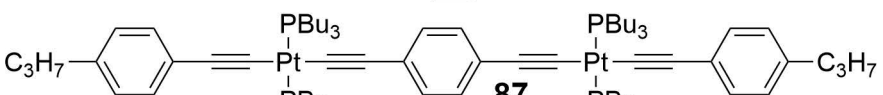

87

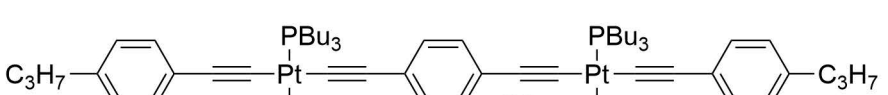

88

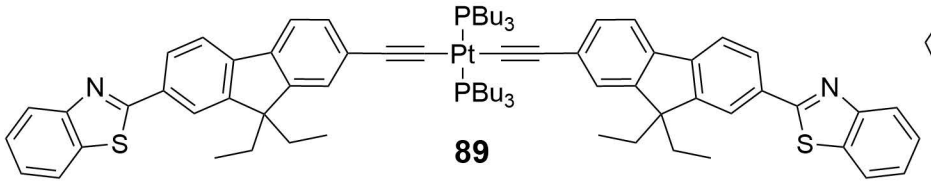

89

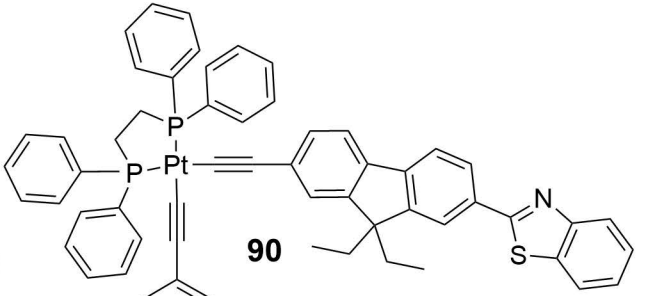

90

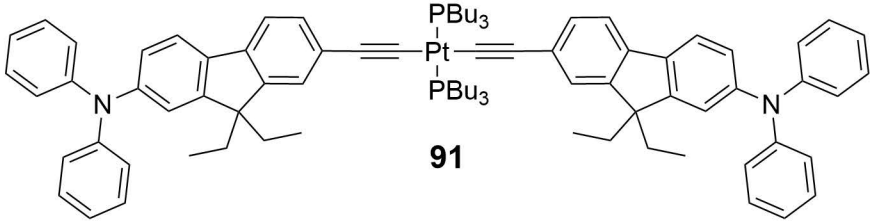

91

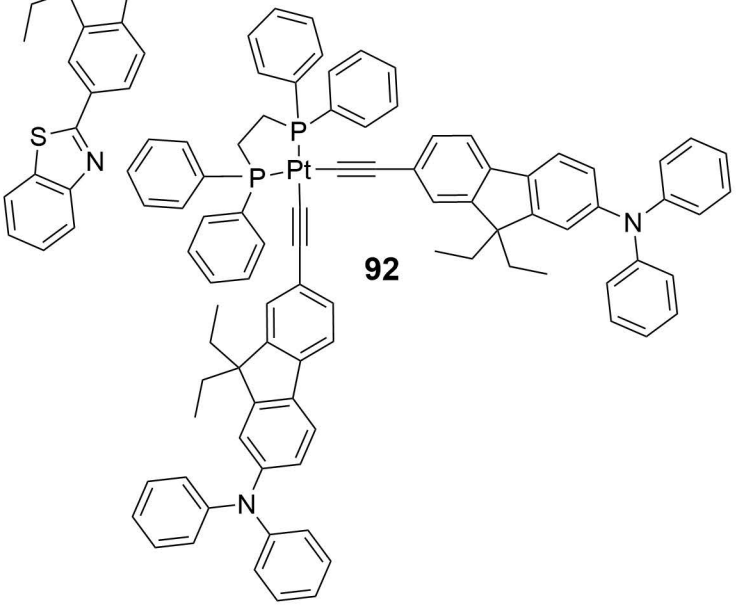

92

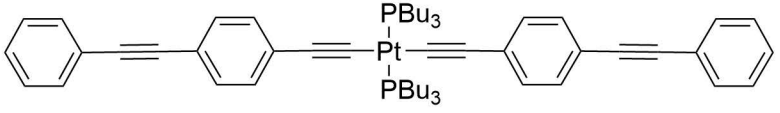

93

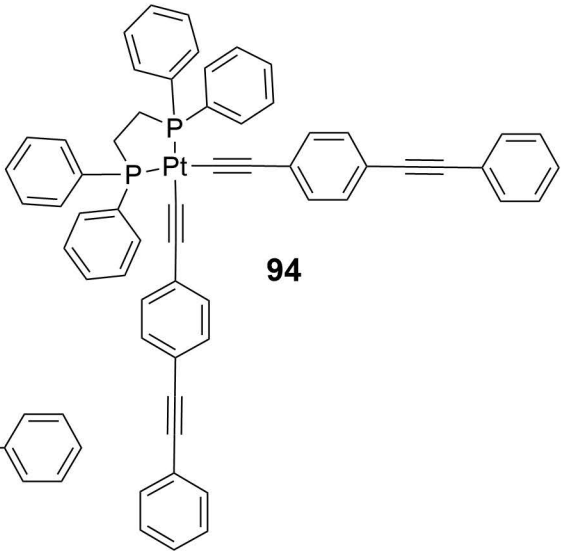

94

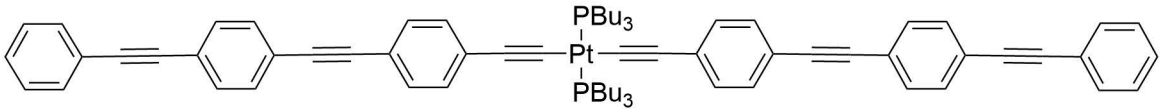

95

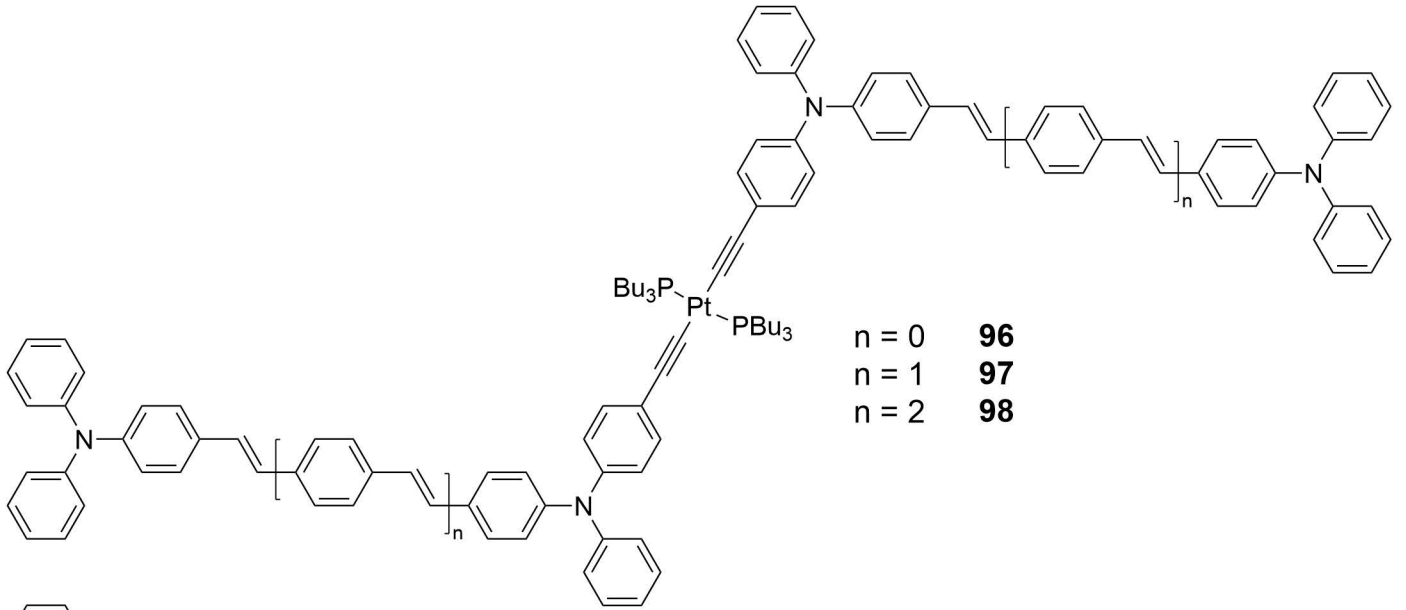

n = 0 **96**
n = 1 **97**
n = 2 **98**

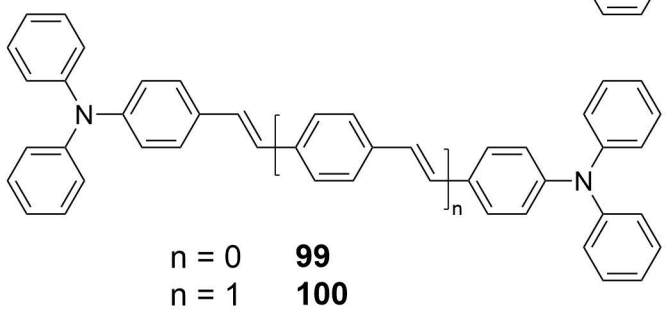

n = 0 **99**
n = 1 **100**
n = 2 **101**

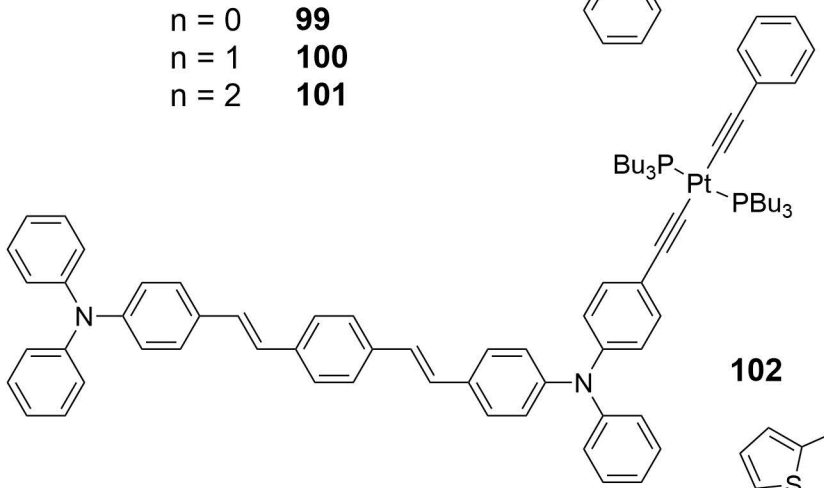

102

103

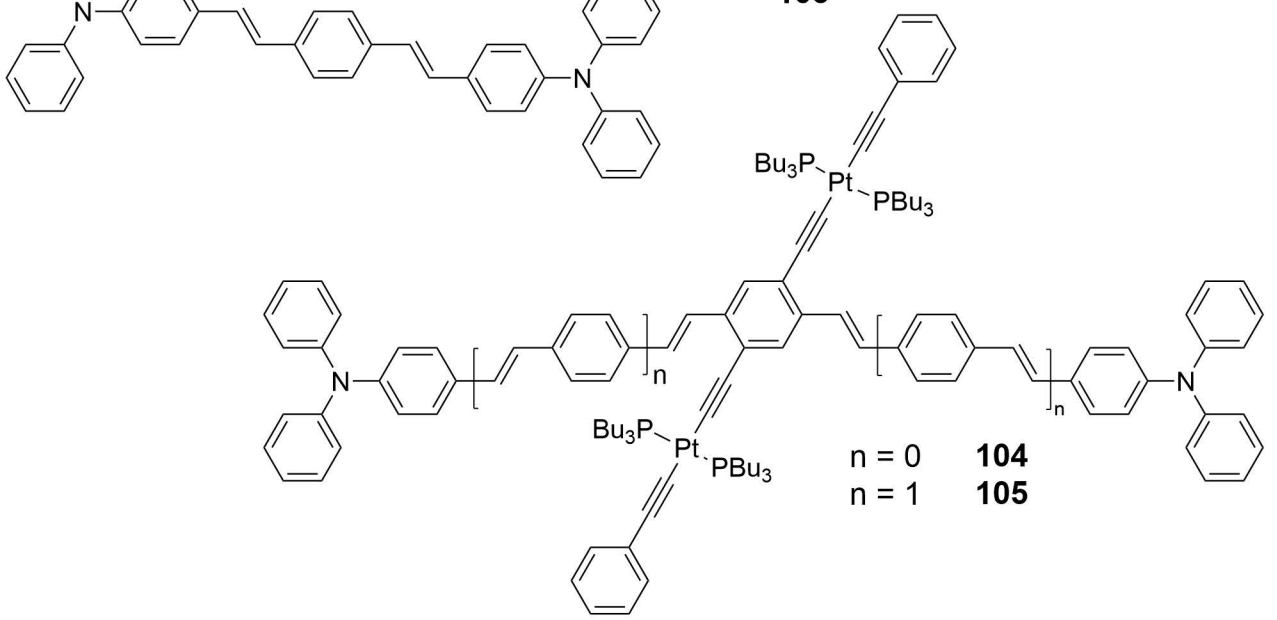

n = 0 **104**
n = 1 **105**

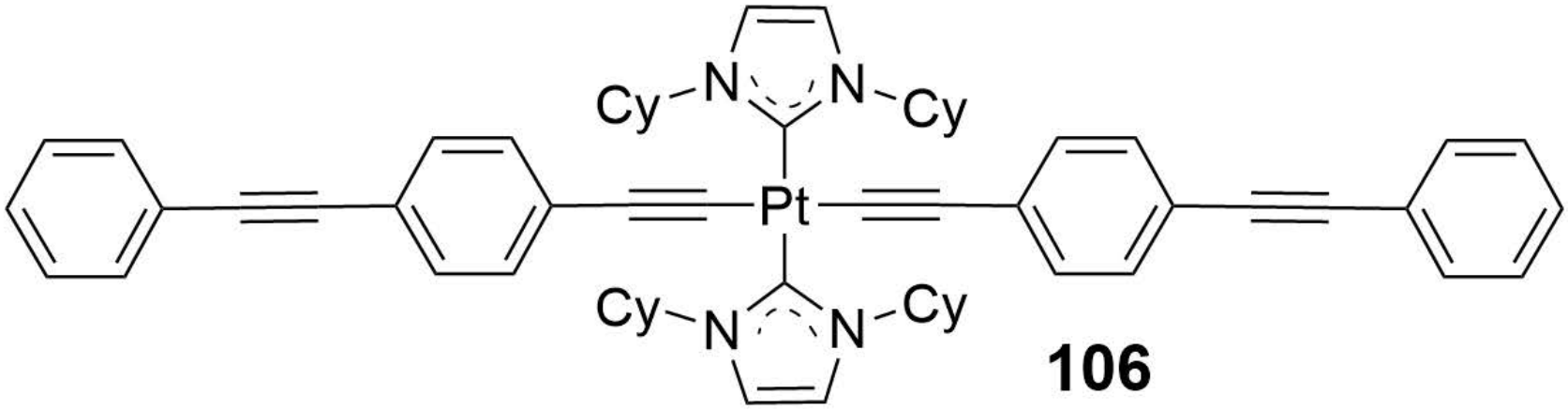

106

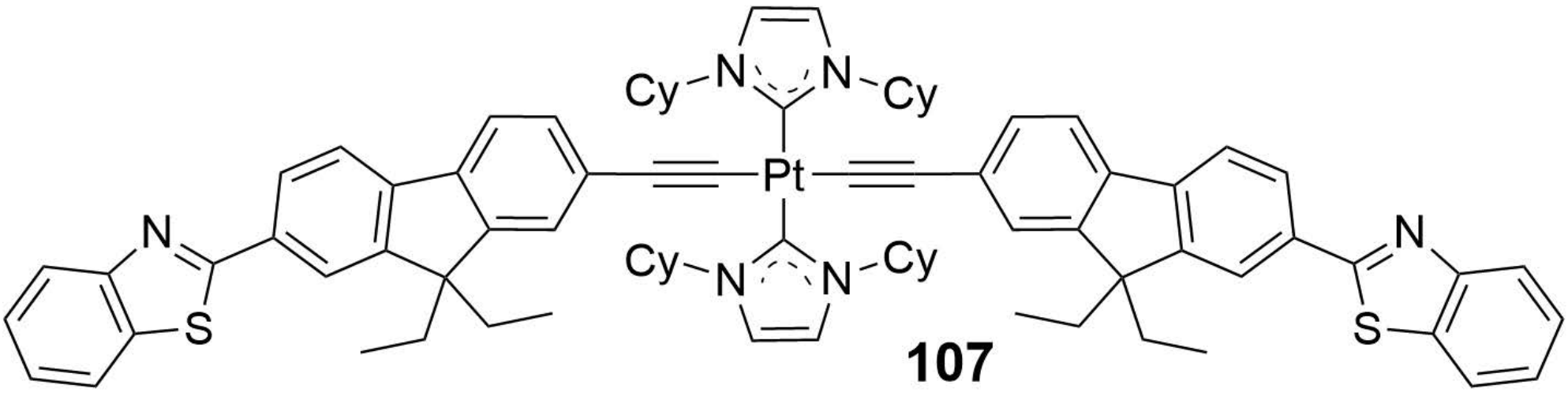

107

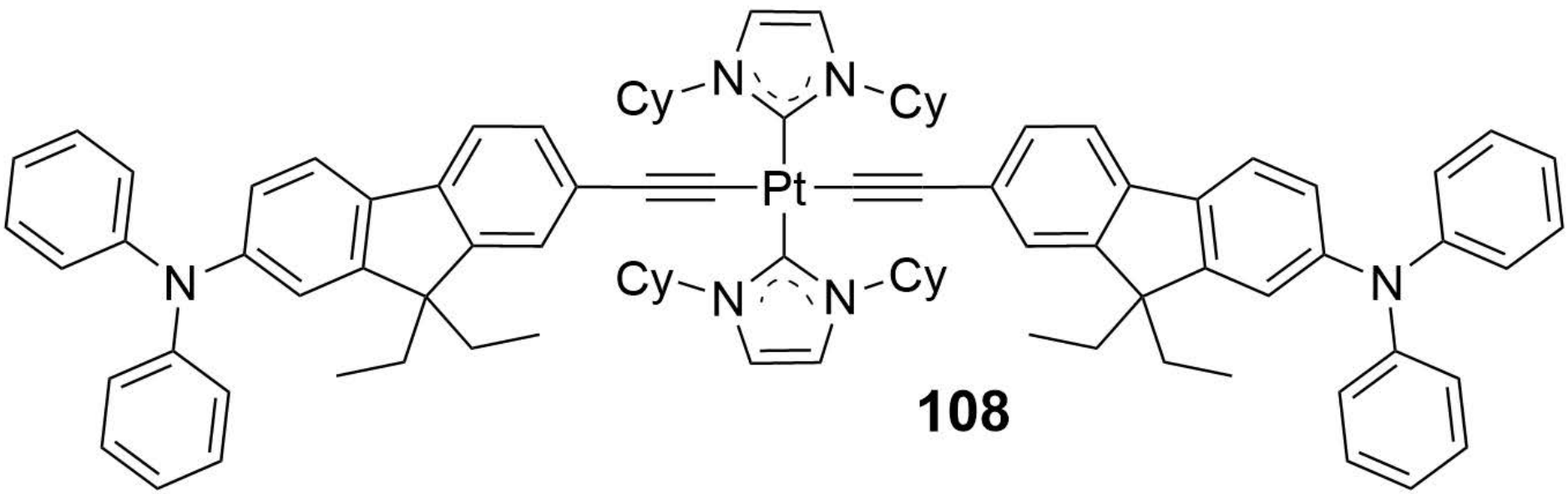

108

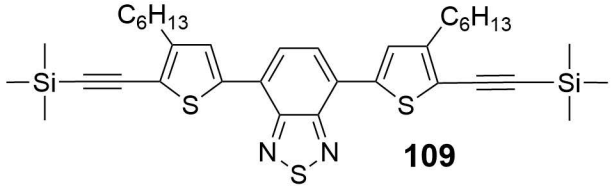

109

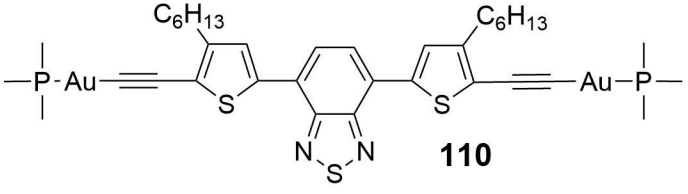

110

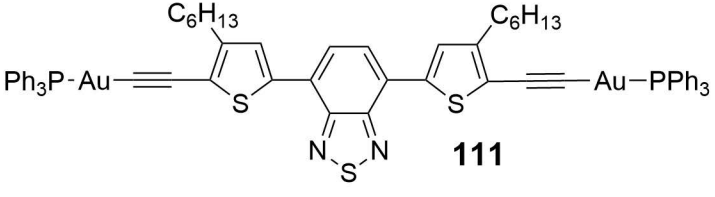

111

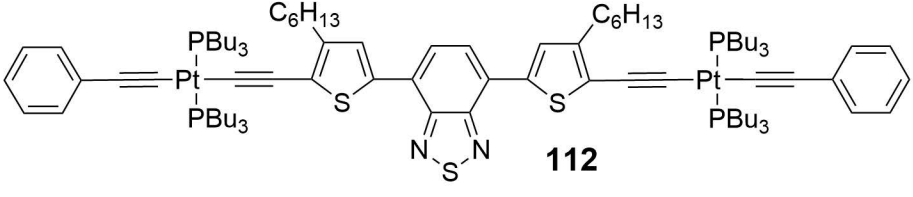

112

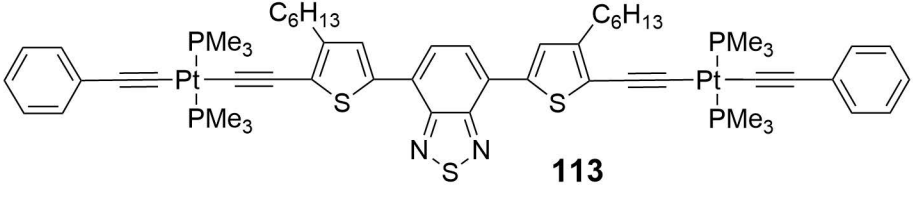

113

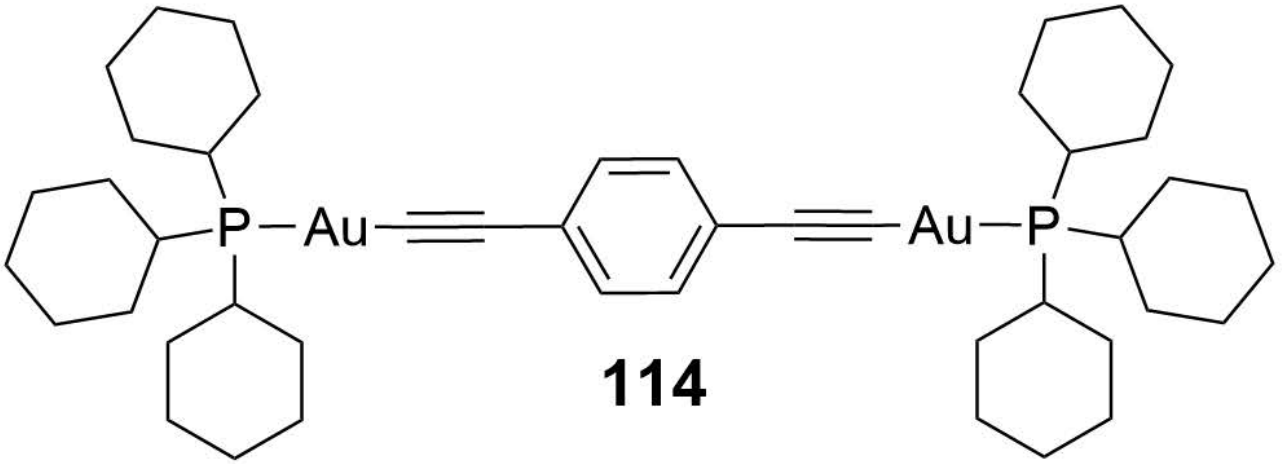

114

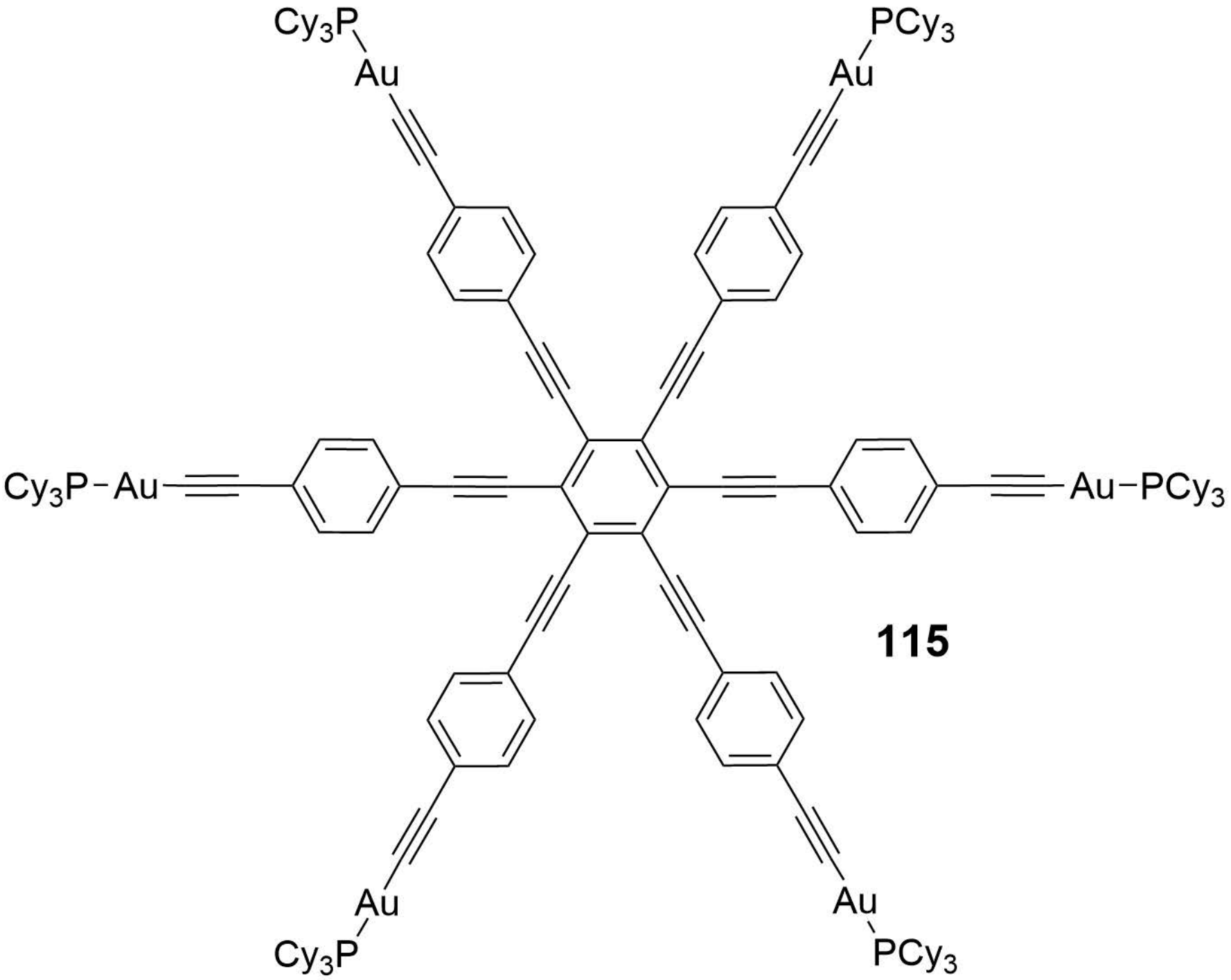

115

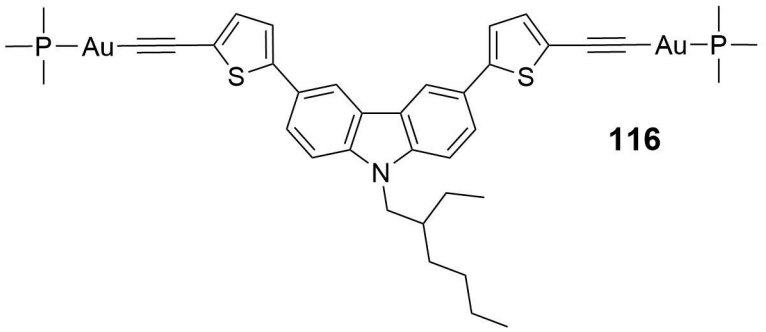

116

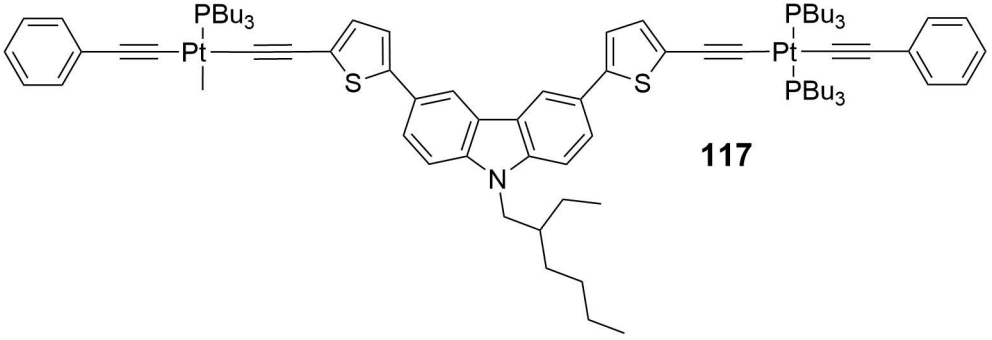

117

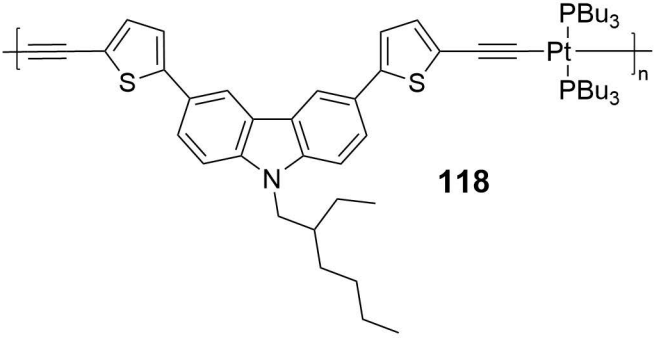

118

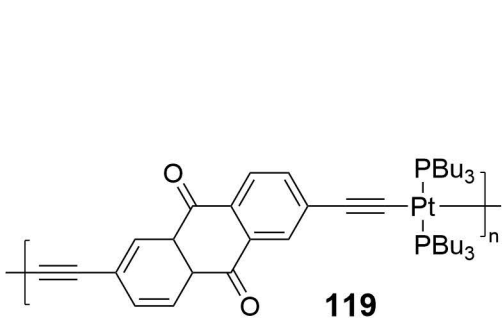
O
O
PBu3
Pt
PBu3
n

119

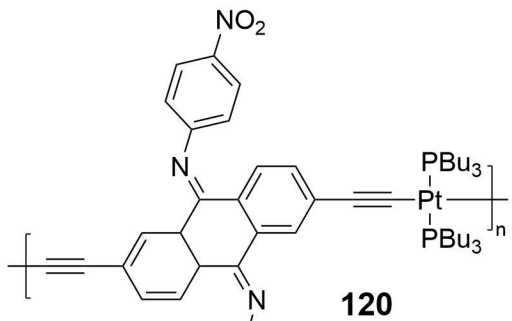
NO2
N
N
O2N
PBu3
Pt
PBu3
n

120

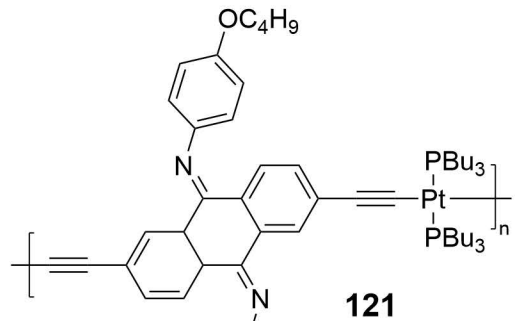
OC4H9
N
N
C4H9O
PBu3
Pt
PBu3
n

121

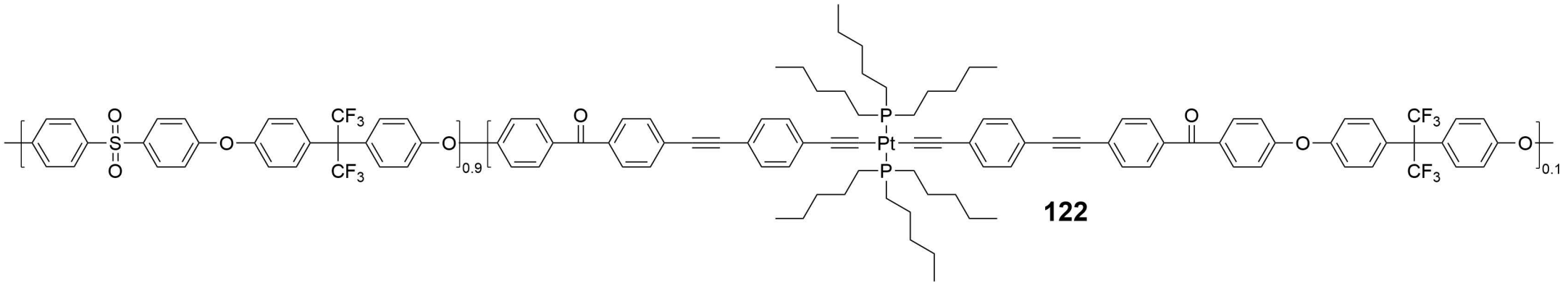

122

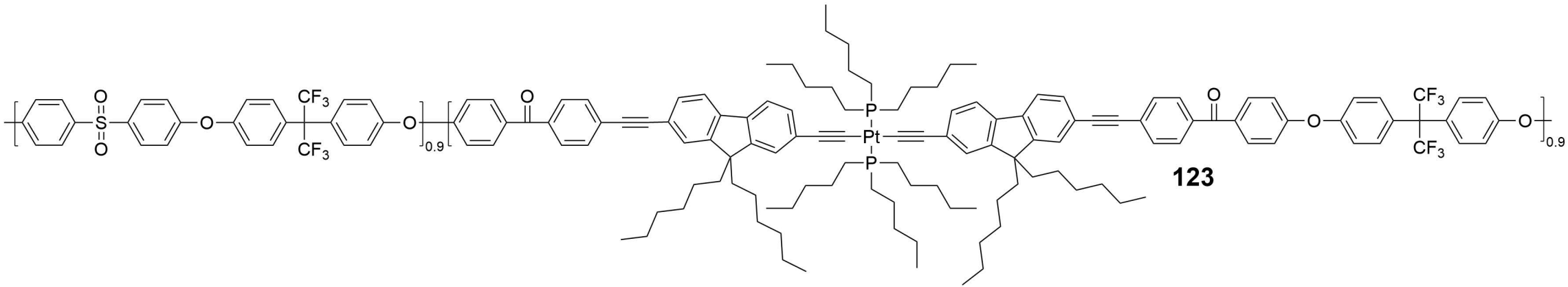

123

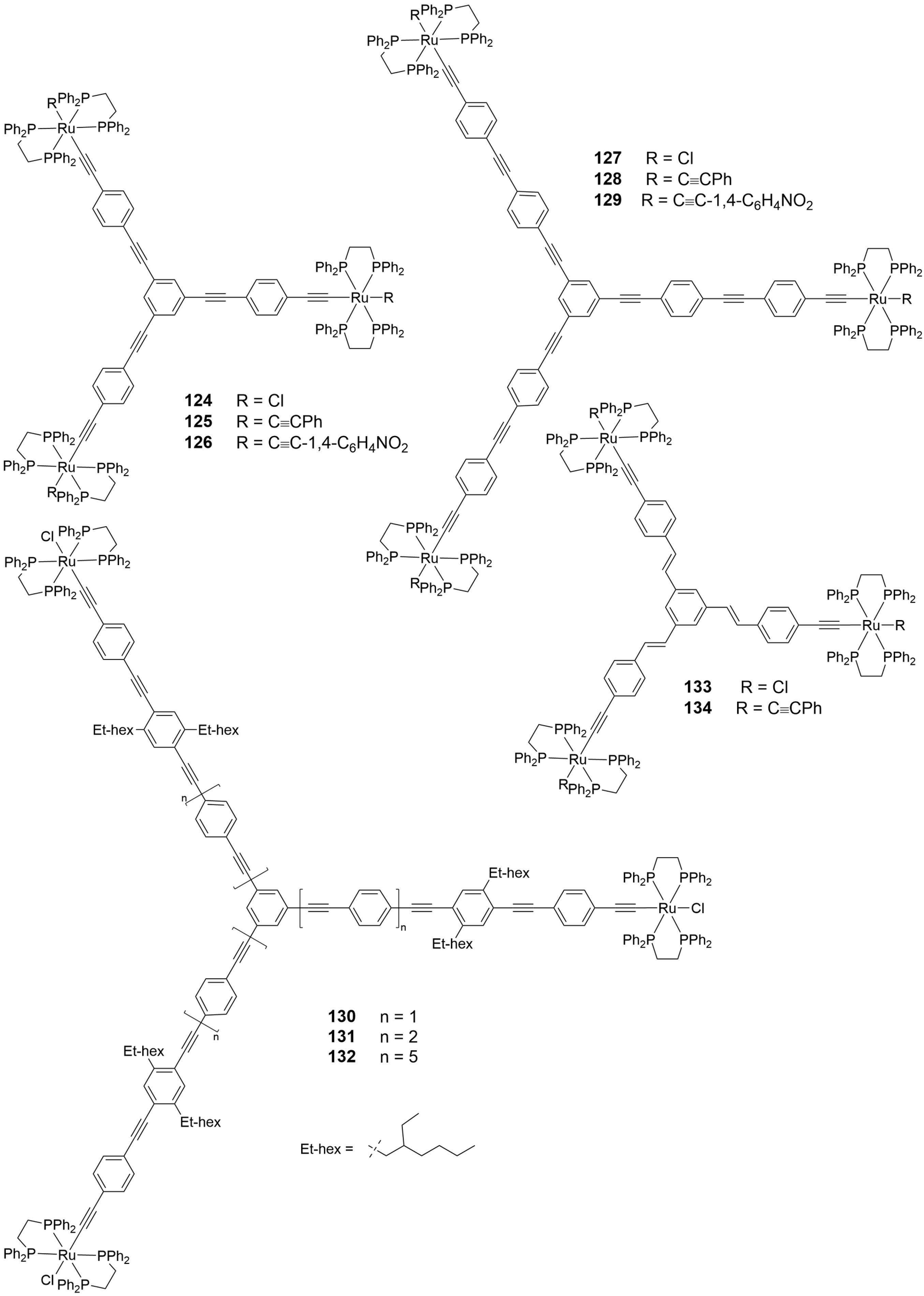
124 R = Cl
125 R = C≡CPh
126 R = C≡C-1,4-C6H4NO2
127 R = Cl
128 R = C≡CPh
129 R = C≡C-1,4-C6H4NO2
133 R = Cl
134 R = C≡CPh
130 n = 1
131 n = 2
132 n = 5
Et-hex
Et-hex =

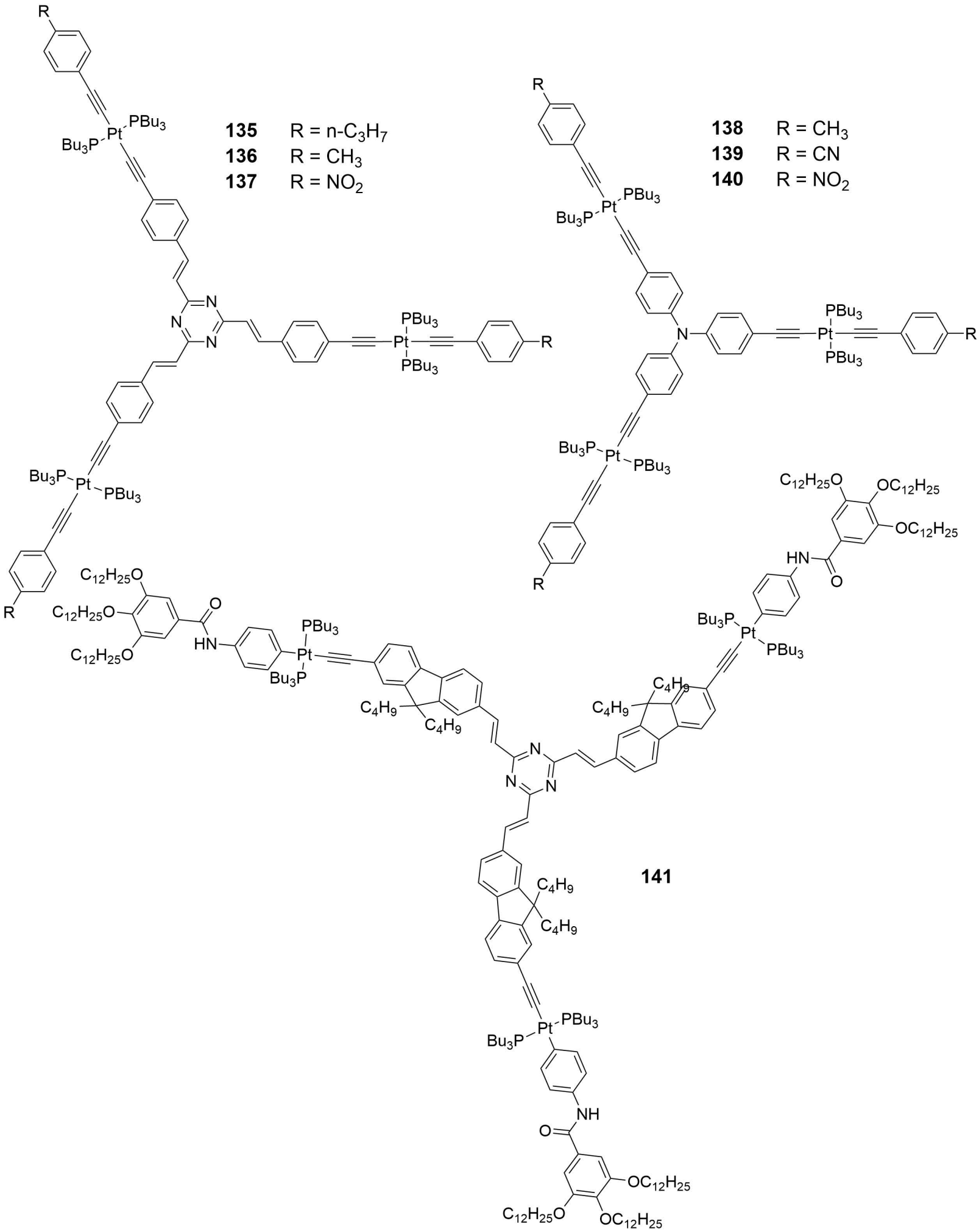
135 R = n-C3H7
136 R = CH3
137 R = NO2
138 R = CH3
139 R = CN
140 R = NO2
141

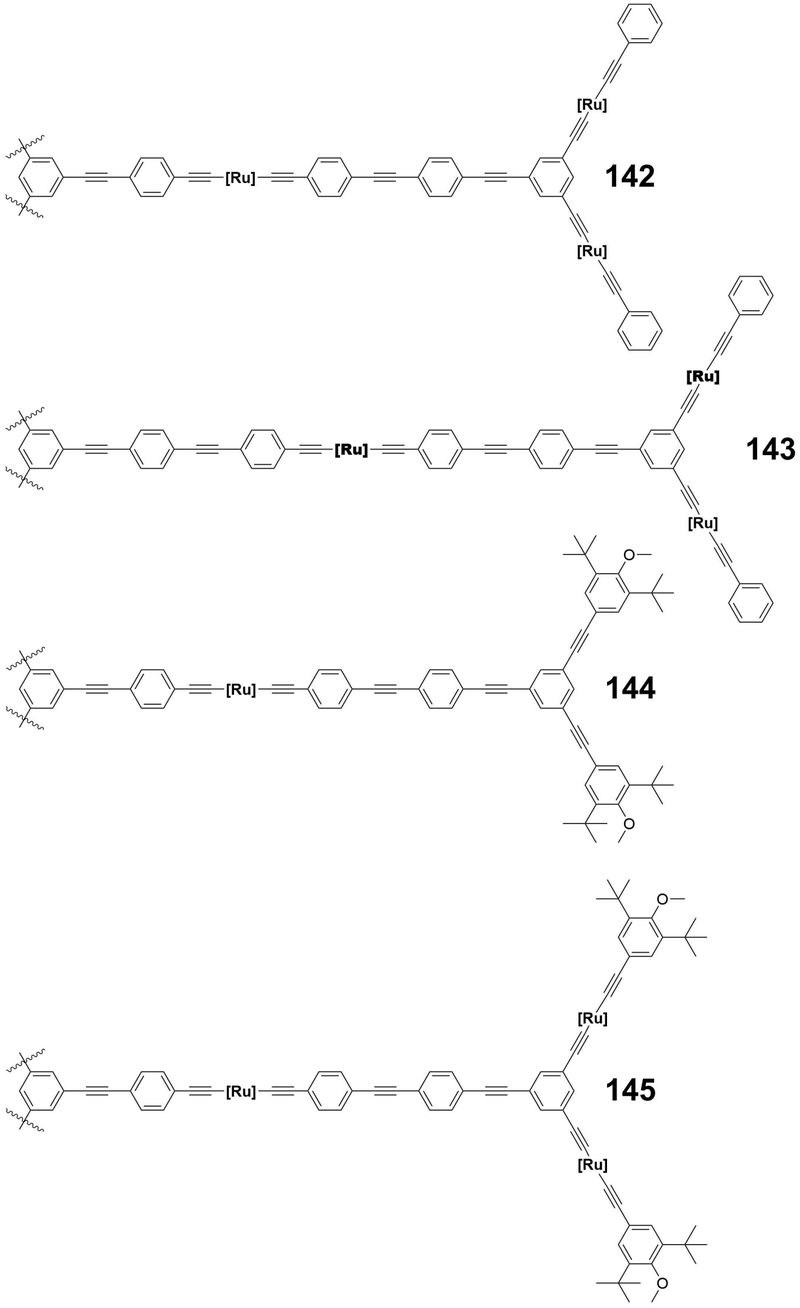
[Ru]
142
143
144
145

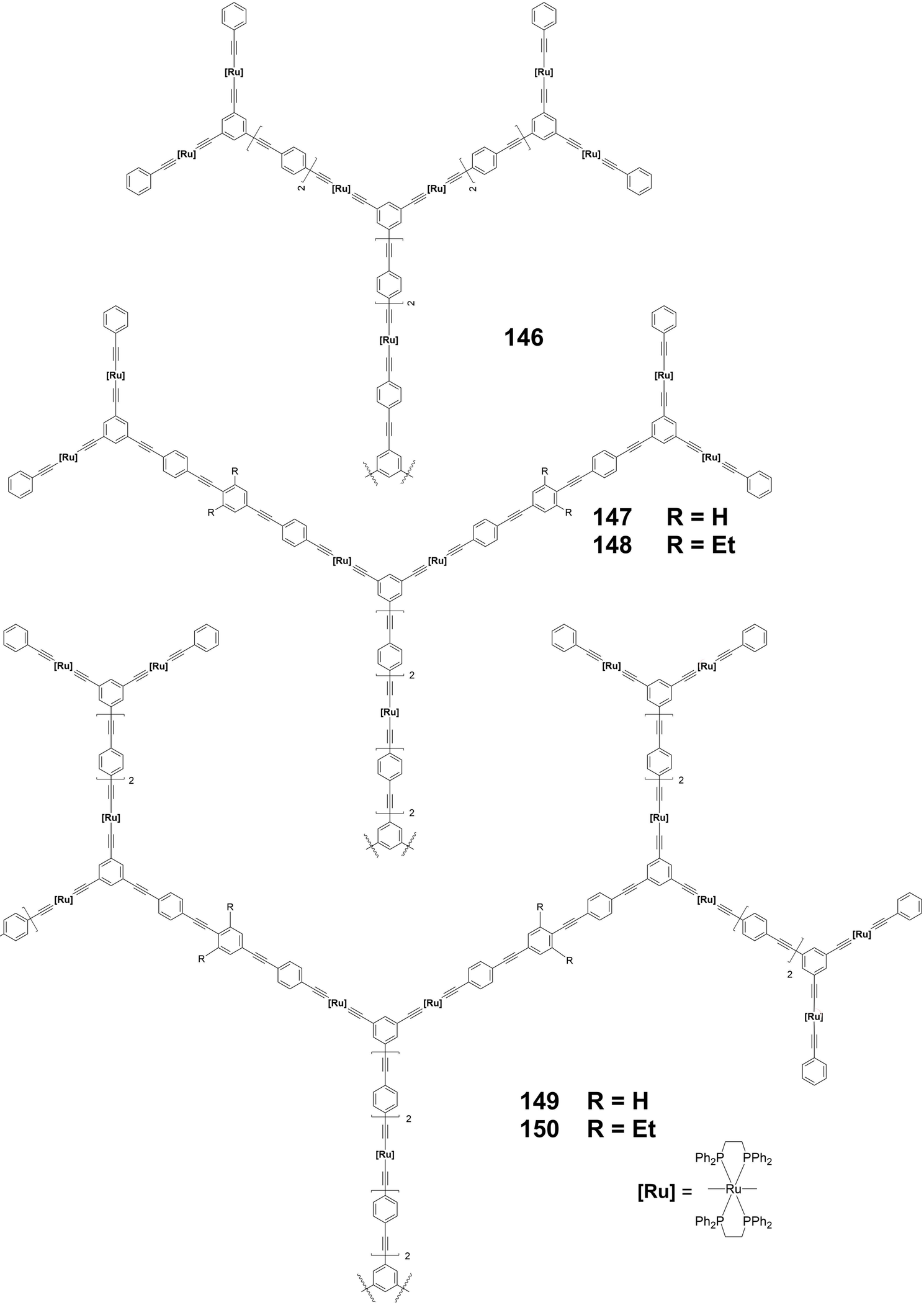
[Ru]
146
147 R = H
148 R = Et
149 R = H
150 R = Et
[Ru] =
Ph2P
PPh2
Ru

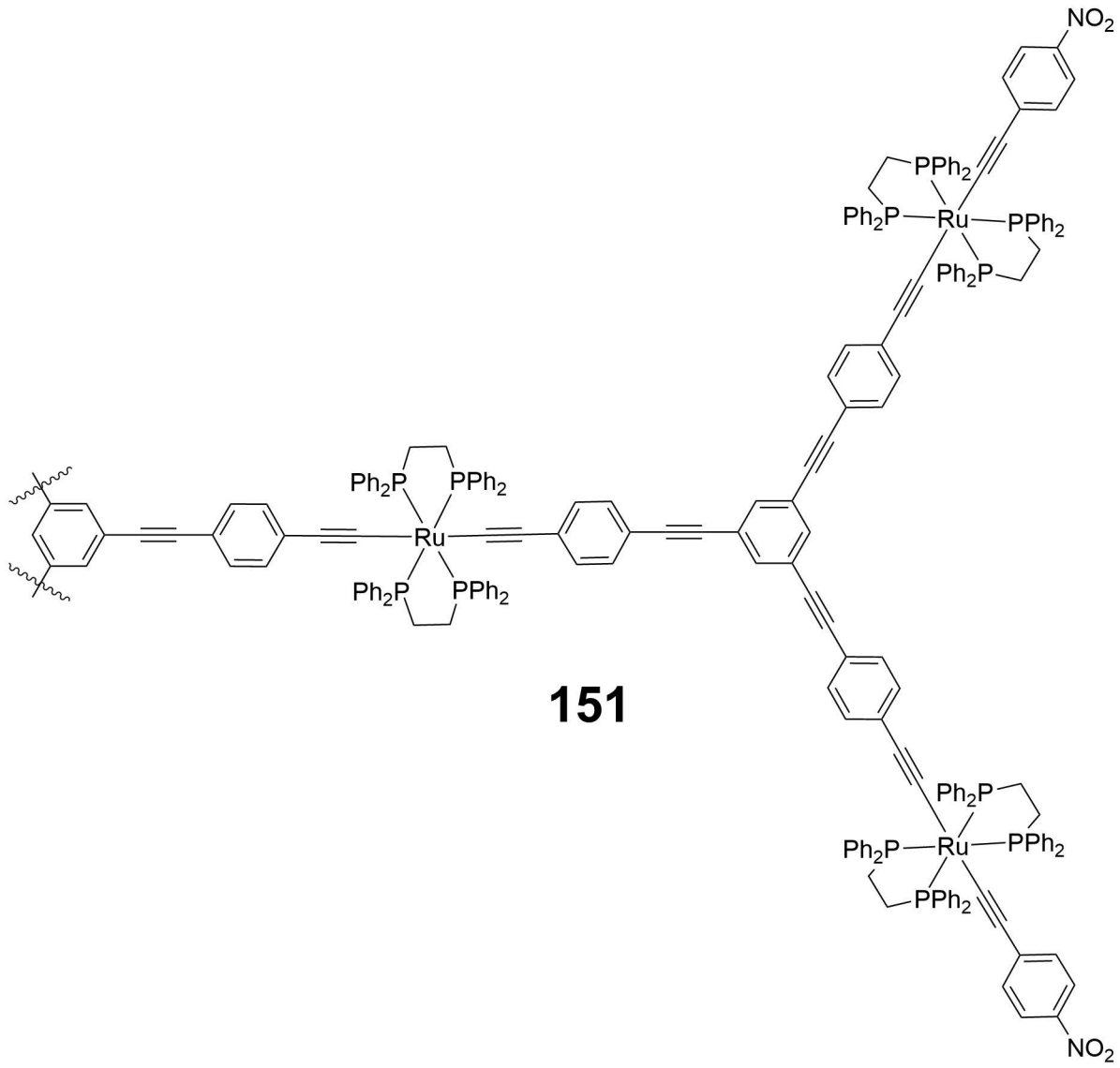
NO2
PPh2
Ph2P
Ru
PPh2
Ph2P
Ph2P
PPh2
Ru
PPh2
Ph2P
Ph2P
PPh2
Ru
PPh2
Ph2P
PPh2
NO2

151